iScience, Volume *24*

Supplemental information

Cholesterol-binding translocator protein TSPO regulates steatosis and bile acid synthesis in nonalcoholic fatty liver disease

Yuchang Li, Liting Chen, Lu Li, Chantal Sottas, Stephanie K. Petrillo, Anthoula Lazaris, Peter Metrakos, Hangyu Wu, Yuji Ishida, Takeshi Saito, Lucy Golden-Mason, Hugo R. Rosen, Jeremy J. Wolff, Cristina I. Silvescu, Samuel Garza, Garett Cheung, Tiffany Huang, Jinjiang Fan, Martine Culty, Bangyan Stiles, Kinji Asahina, and Vassilios Papadopoulos

Figure S1

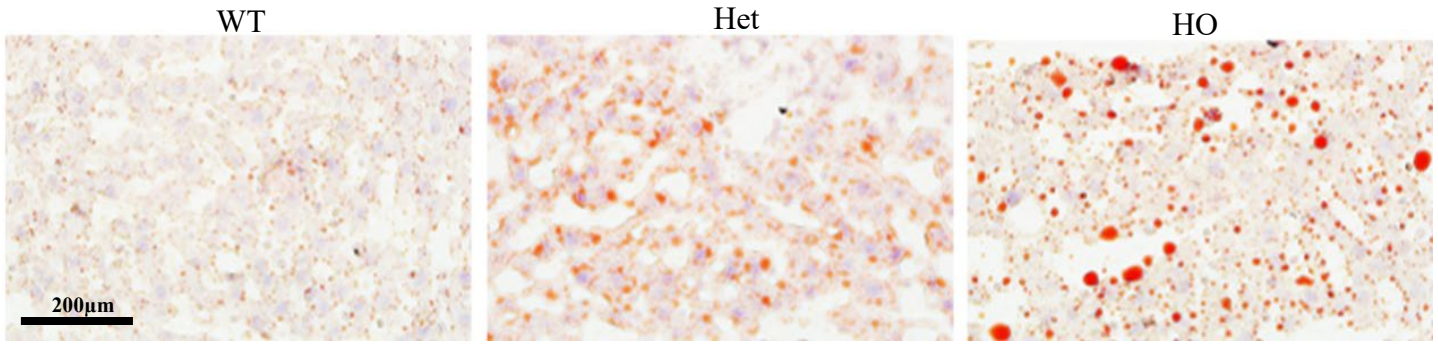

Figure S2

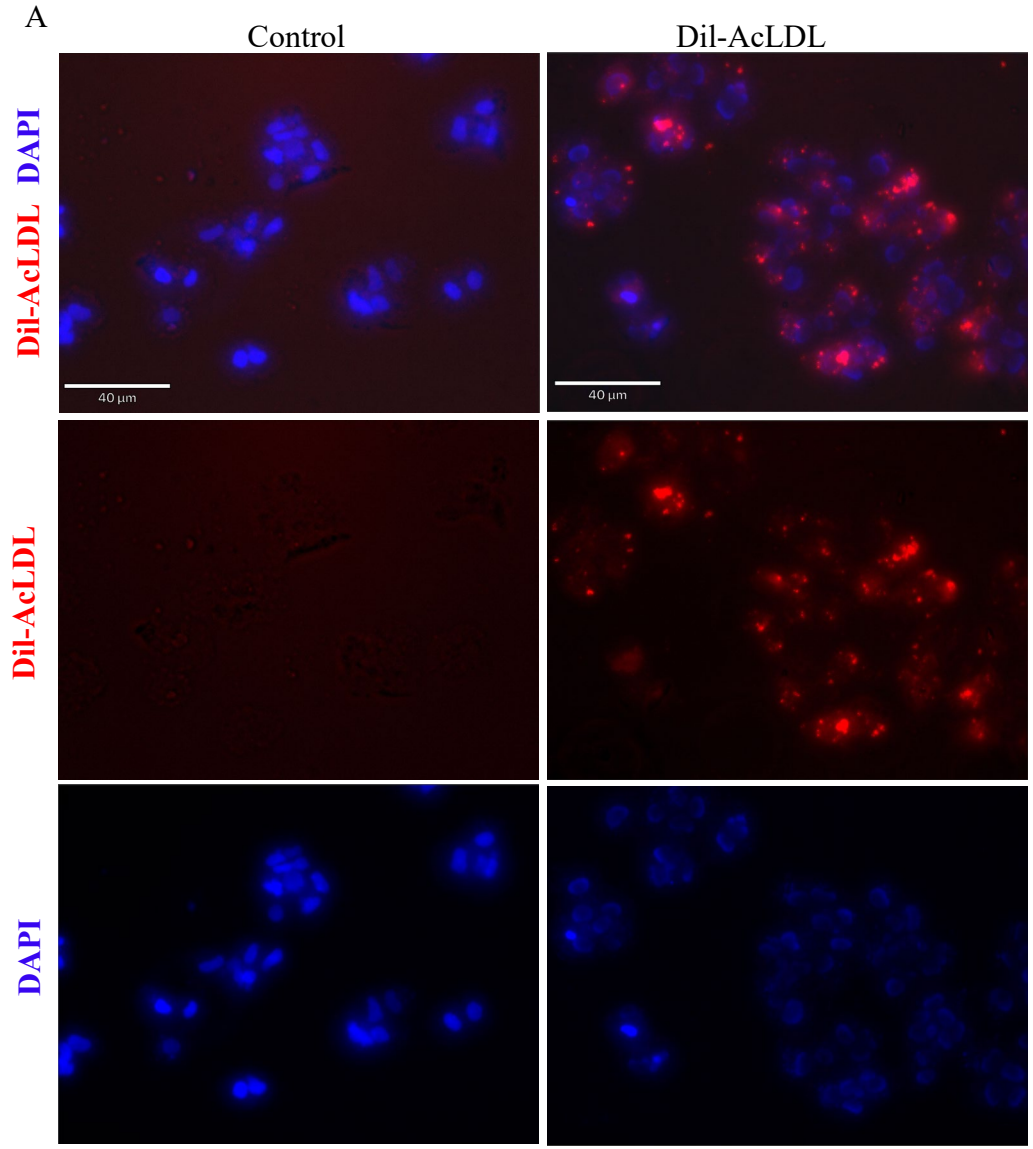
A
Control
Dil-AcLDL
Dil-AcLDL DAPI
Dil-AcLDL
DAPI
40 μm
40 μm

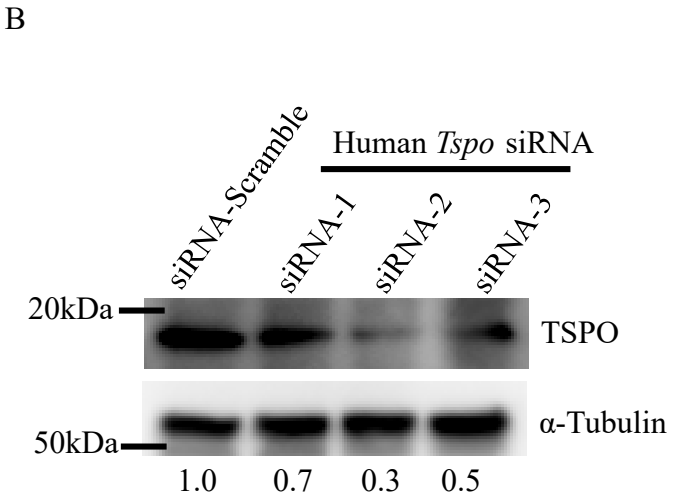
B
Human Tspo siRNA
siRNA-Scramble
siRNA-1
siRNA-2
siRNA-3
20kDa
TSPO
50kDa
α-Tubulin
1.0
0.7
0.3
0.5

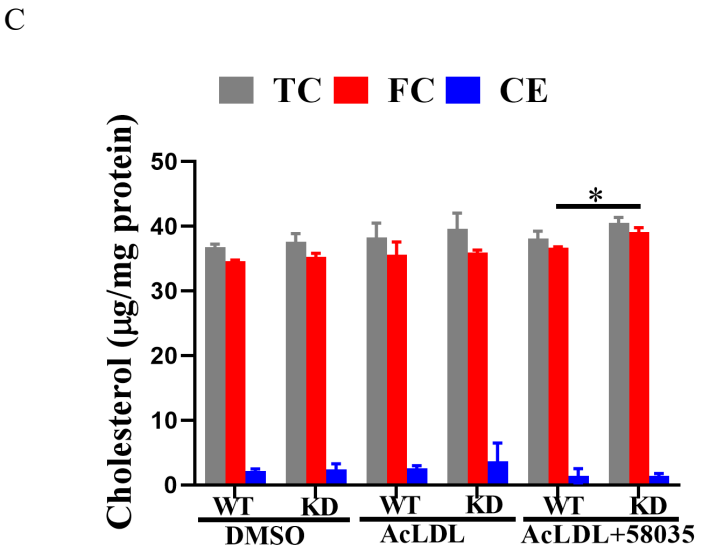
C
TC
FC
CE
Cholesterol (μg/mg protein)
50
40
30
20
10
0
*
WT
KD
WT
KD
WT
KD
DMSO
AcLDL
AcLDL+58035

Figure S3

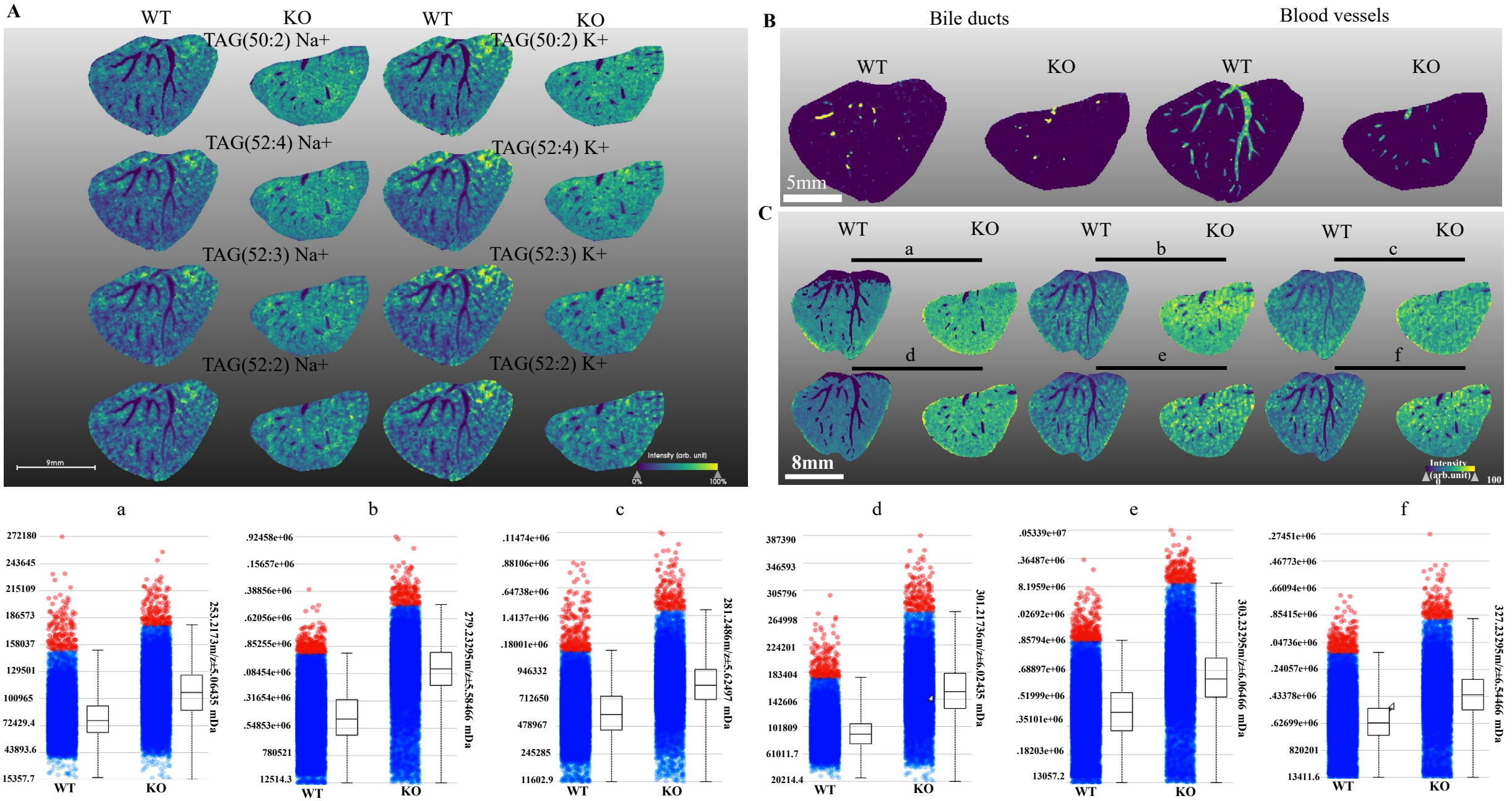
A
WT
KO
WT
KO
TAG(50:2) Na+
TAG(50:2) K+
TAG(52:4) Na+
TAG(52:4) K+
TAG(52:3) Na+
TAG(52:3) K+
TAG(52:2) Na+
TAG(52:2) K+
9mm
Intensity (arb. unit)
0%
100%
B
Bile ducts
Blood vessels
WT
KO
WT
KO
5mm
C
WT
KO
WT
KO
WT
KO
a
b
c
d
e
f
8mm
Intensity (arb.unit)
100
a
272180
243645
215109
186573
158037
129501
100965
72429.4
43893.6
15357.7
WT
KO
253.2173m/z±5.06435 mDa
b
.92458e+06
.15657e+06
.38856e+06
.62056e+06
.85255e+06
.08454e+06
.31654e+06
.54853e+06
780521
12514.3
WT
KO
279.23295m/z±5.58466 mDa
c
.11474e+06
.88106e+06
.64738e+06
1.4137e+06
.18001e+06
946332
712650
478967
245285
11602.9
WT
KO
281.2486m/z±5.62497 mDa
d
387390
346593
305796
264998
224201
183404
142606
101809
61011.7
20214.4
WT
KO
301.21736m/z±6.02435 mDa
e
.05339e+07
.36487e+06
8.1959e+06
.02692e+06
.85794e+06
.68897e+06
.51999e+06
.35101e+06
.18203e+06
13057.2
WT
KO
303.23295m/z±6.06466 mDa
f
.27451e+06
.46773e+06
.66094e+06
.85415e+06
.04736e+06
.24057e+06
.43378e+06
.62699e+06
820201
13411.6
WT
KO
327.23295m/z±6.54466 mDa

Figure S4

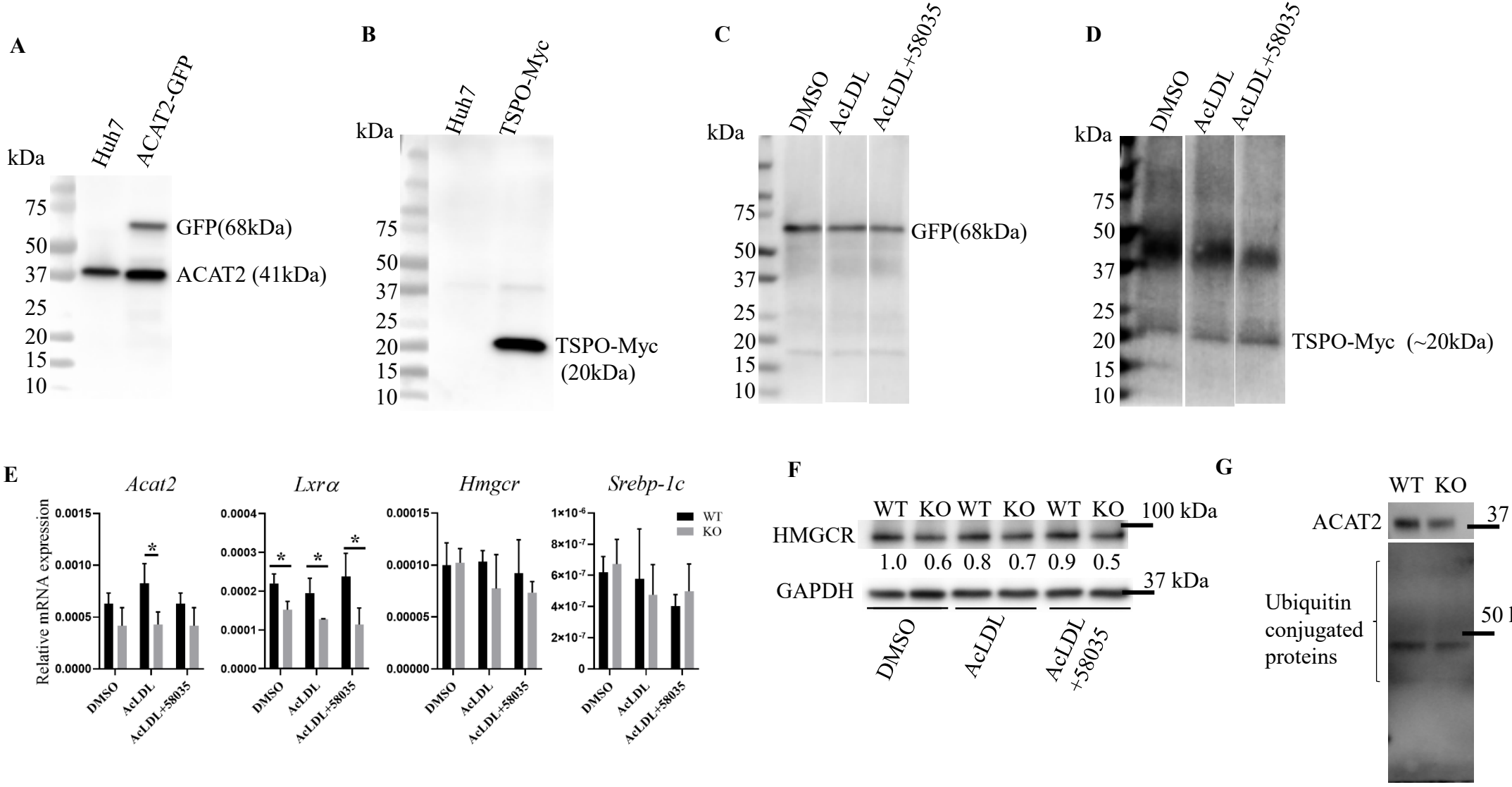
A
Huh7
ACAT2-GFP
kDa
75
50
37
25
20
15
10
GFP(68kDa)
ACAT2 (41kDa)
B
Huh7
TSPO-Myc
kDa
75
50
37
25
20
15
10
TSPO-Myc
(20kDa)
C
DMSO
AcLDL
AcLDL+58035
kDa
75
50
37
25
20
15
10
GFP(68kDa)
D
DMSO
AcLDL
AcLDL+58035
kDa
75
50
37
25
20
15
10
TSPO-Myc (~20kDa)
E
Acat2
Lxrα
Hmgcr
Srebp-1c
Relative mRNA expression
WT
KO
DMSO
AcLDL
AcLDL+58035
F
WT KO WT KO WT KO
100 kDa
HMGCR
1.0 0.6 0.8 0.7 0.9 0.5
GAPDH
37 kDa
DMSO
AcLDL
AcLDL +58035
G
WT KO
ACAT2
37 kDa
Ubiquitin conjugated proteins
50 kDa

Figure S5

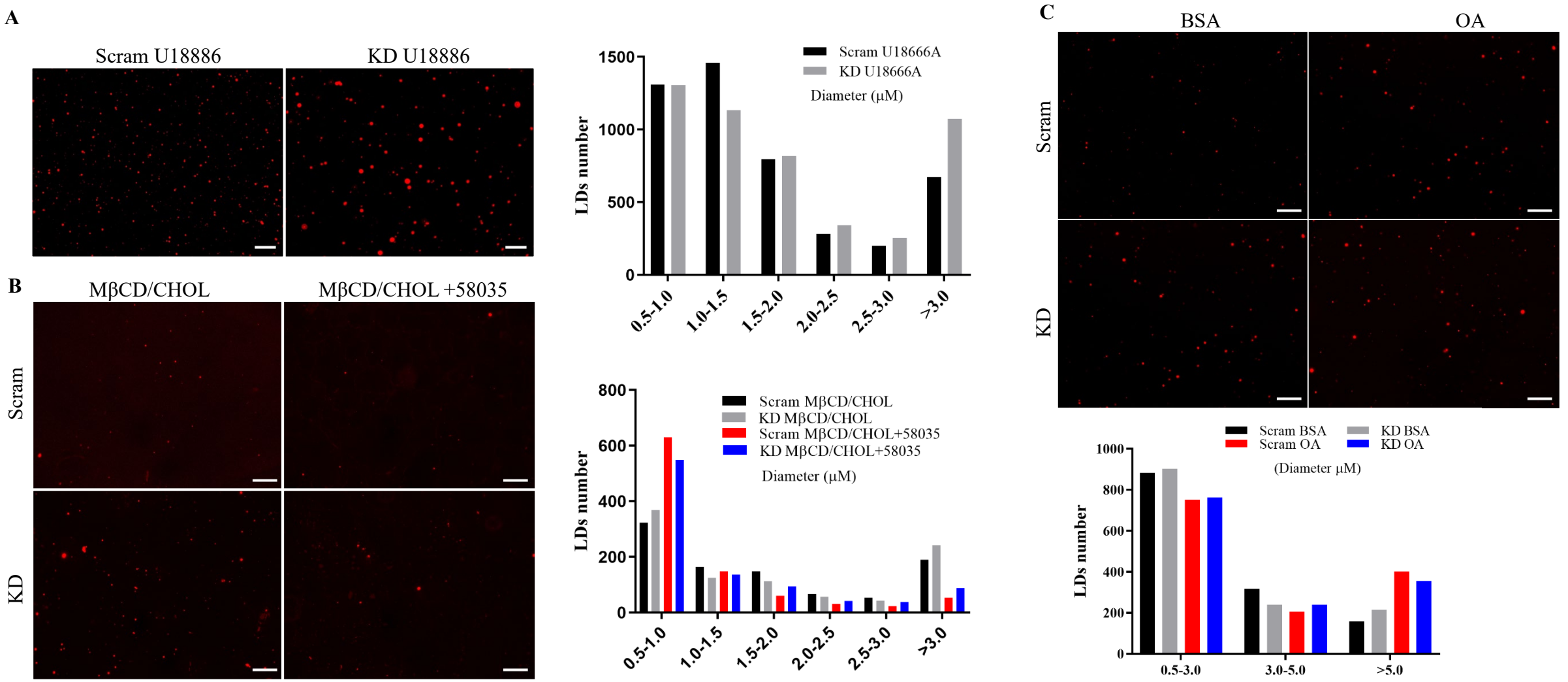
A
Scram U18886
KD U18886
B
MβCD/CHOL
MβCD/CHOL +58035
Scram
KD
Scram U18666A
KD U18666A
Diameter (μM)
LDs number
1500
1000
500
0
0.5-1.0
1.0-1.5
1.5-2.0
2.0-2.5
2.5-3.0
>3.0
Scram MβCD/CHOL
KD MβCD/CHOL
Scram MβCD/CHOL+58035
KD MβCD/CHOL+58035
Diameter (μM)
LDs number
800
600
400
200
0
C
BSA
OA
Scram
KD
Scram BSA
KD BSA
Scram OA
KD OA
(Diameter μM)
LDs number
1000
800
600
400
200
0
0.5-3.0
3.0-5.0
>5.0

Figure S6

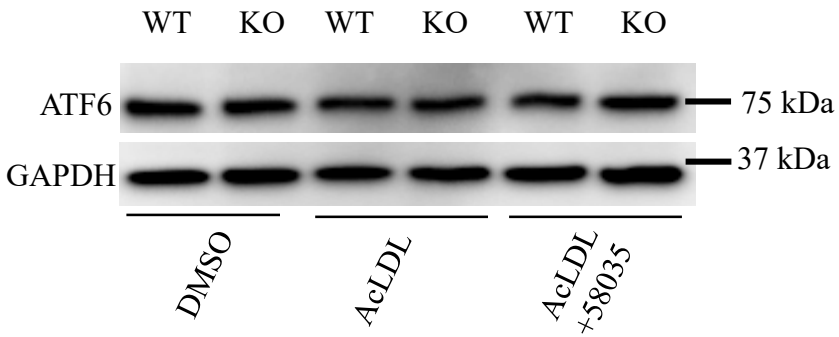
WT
KO
WT
KO
WT
KO
ATF6
75 kDa
GAPDH
37 kDa
DMSO
AcLDL
AcLDL +58035

Figure S7

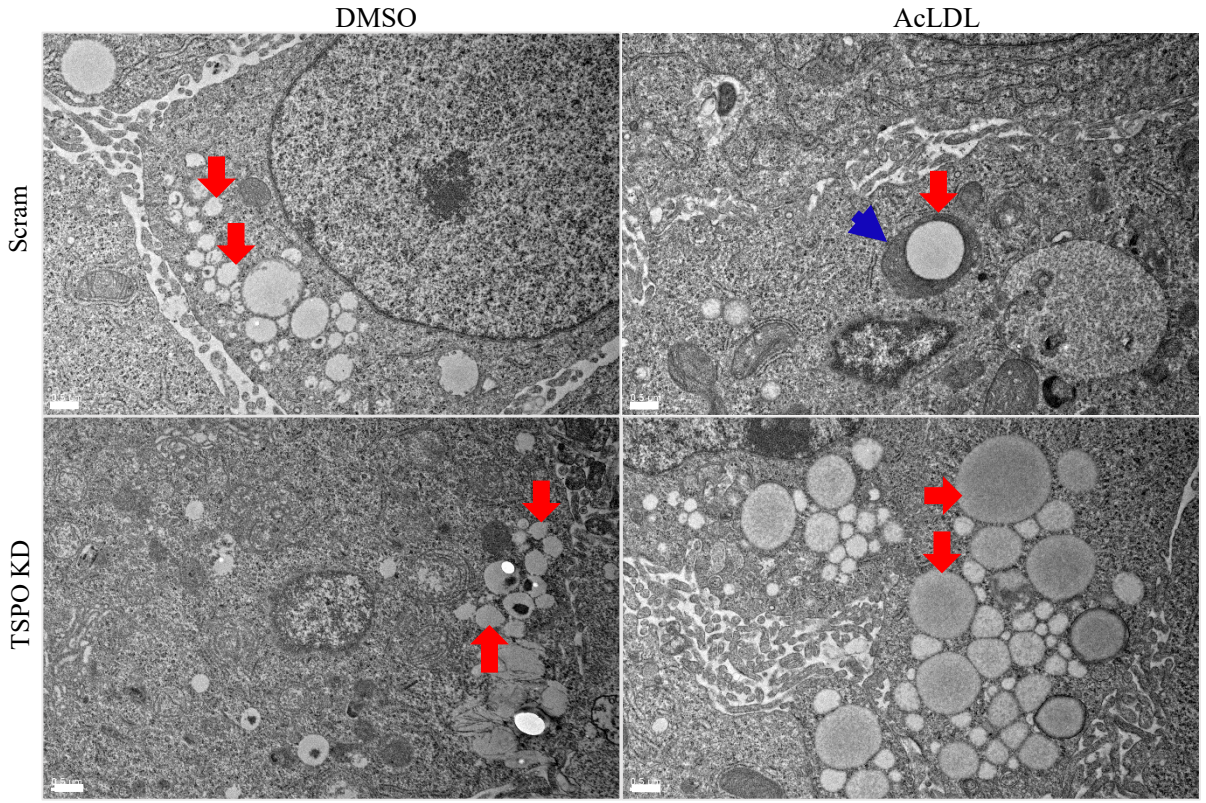

Figure S8

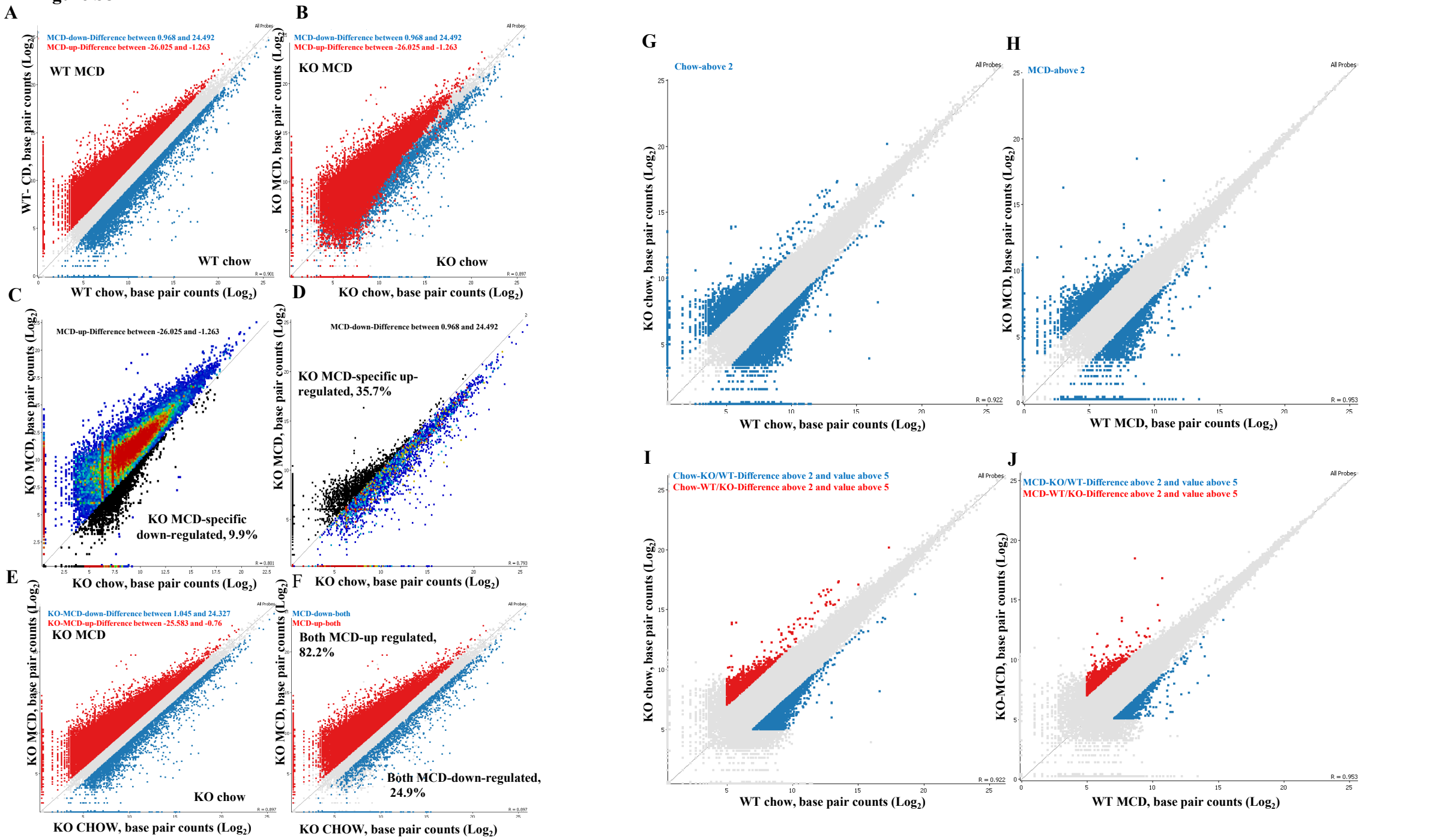
A
MCD-down-Difference between 0.968 and 24.492
MCD-up-Difference between -26.025 and -1.263
WT MCD
WT chow
WT- CD, base pair counts (Log2)
WT chow, base pair counts (Log2)
B
MCD-down-Difference between 0.968 and 24.492
MCD-up-Difference between -26.025 and -1.263
KO MCD
KO chow
KO MCD, base pair counts (Log2)
KO chow, base pair counts (Log2)
C
MCD-up-Difference between -26.025 and -1.263
KO MCD-specific down-regulated, 9.9%
KO MCD, base pair counts (Log2)
KO chow, base pair counts (Log2)
D
MCD-down-Difference between 0.968 and 24.492
KO MCD-specific up-regulated, 35.7%
KO MCD, base pair counts (Log2)
KO chow, base pair counts (Log2)
E
KO-MCD-down-Difference between 1.045 and 24.327
KO-MCD-up-Difference between -25.583 and -0.76
KO MCD
KO chow
KO MCD, base pair counts (Log2)
KO CHOW, base pair counts (Log2)
F
MCD-down-both
MCD-up-both
Both MCD-up regulated, 82.2%
Both MCD-down-regulated, 24.9%
KO MCD, base pair counts (Log2)
KO CHOW, base pair counts (Log2)
G
Chow-above 2
KO chow, base pair counts (Log2)
WT chow, base pair counts (Log2)
H
MCD-above 2
KO MCD, base pair counts (Log2)
WT MCD, base pair counts (Log2)
I
Chow-KO/WT-Difference above 2 and value above 5
Chow-WT/KO-Difference above 2 and value above 5
KO chow, base pair counts (Log2)
WT chow, base pair counts (Log2)
J
MCD-KO/WT-Difference above 2 and value above 5
MCD-WT/KO-Difference above 2 and value above 5
KO-MCD, base pair counts (Log2)
WT MCD, base pair counts (Log2)

Figure S9

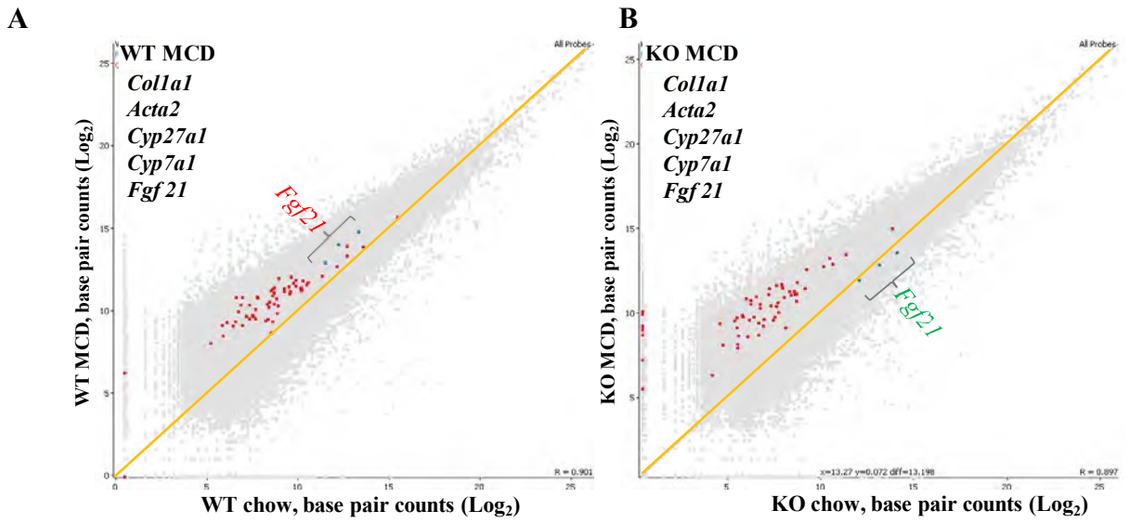
A
WT MCD
Col1a1
Acta2
Cyp27a1
Cyp7a1
Fgf 21
Fgf21
All Probes
WT MCD, base pair counts (Log2)
WT chow, base pair counts (Log2)
R = 0.901
B
KO MCD
Col1a1
Acta2
Cyp27a1
Cyp7a1
Fgf 21
Fgf21
All Probes
KO MCD, base pair counts (Log2)
KO chow, base pair counts (Log2)
R = 0.897

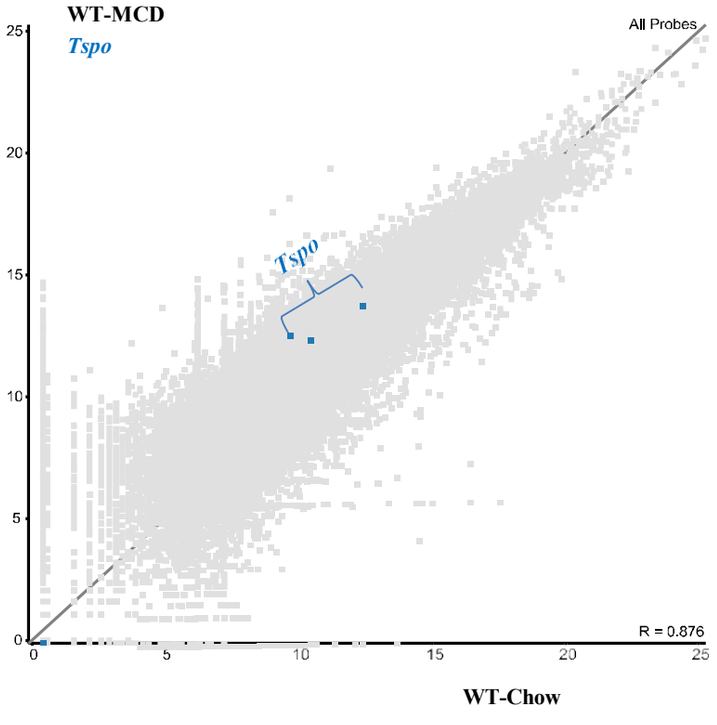
C
WT-MCD
Tspo
All Probes
R = 0.876
WT-Chow

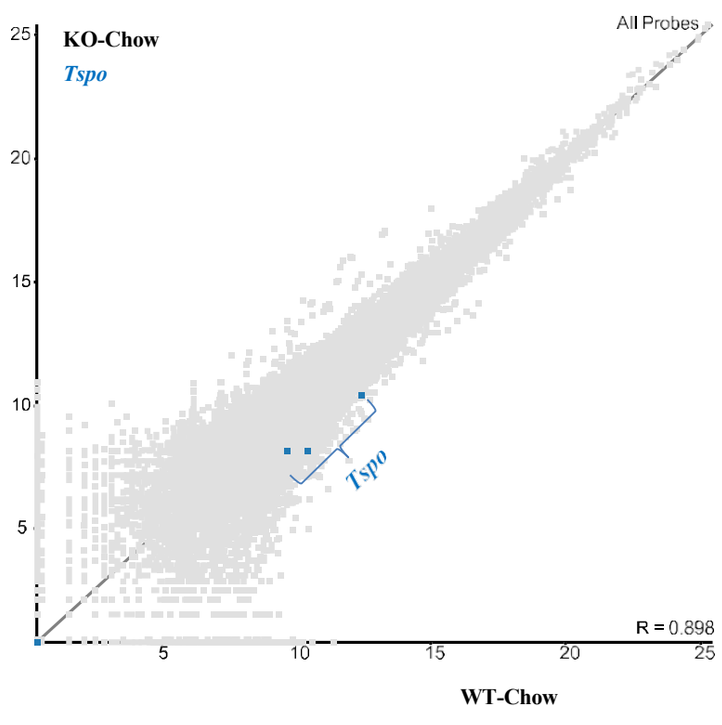
D
KO-Chow
Tspo
All Probes
R = 0.898
WT-Chow

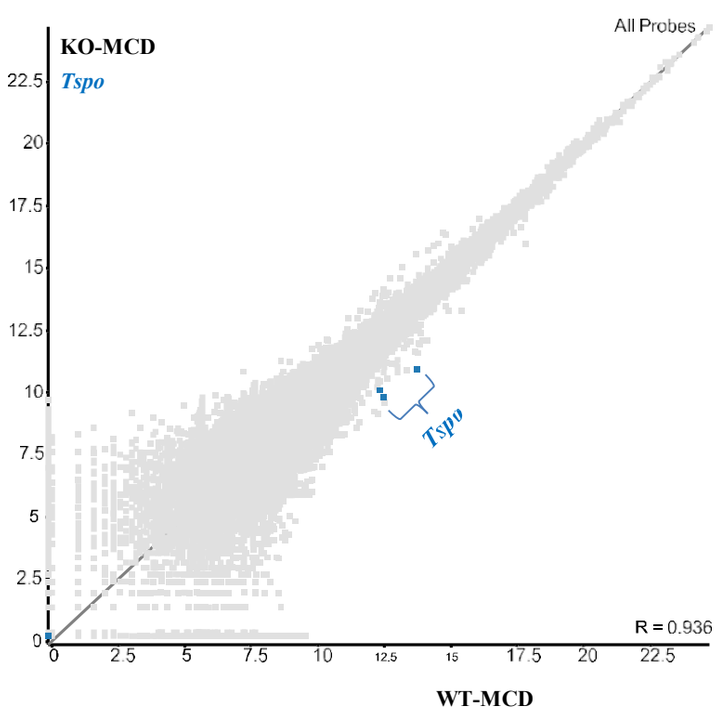
E
KO-MCD
Tspo
All Probes
R = 0.936
WT-MCD

Figure S10

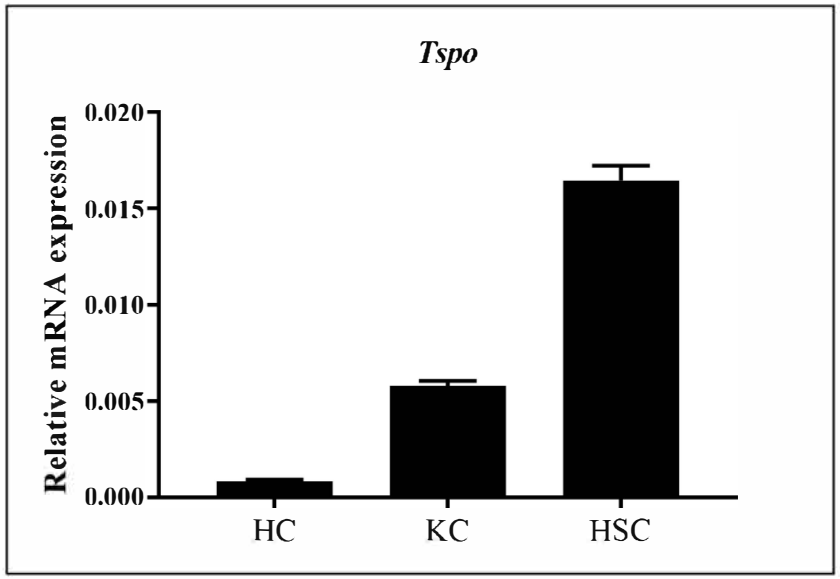
Tspo
Relative mRNA expression
0.020
0.015
0.010
0.005
0.000
HC
KC
HSC

Figure S11

A TSPO conserved peptide

Mus musculus	WRDNHGWRGGRRLPE
Mus Pahari	WRDNSGRRGGSRLPE
Human	WRDNSGRRGGSRLAE
Rat	WRDNSGRRGGSRLTE
	* * * * * * * * * ** *

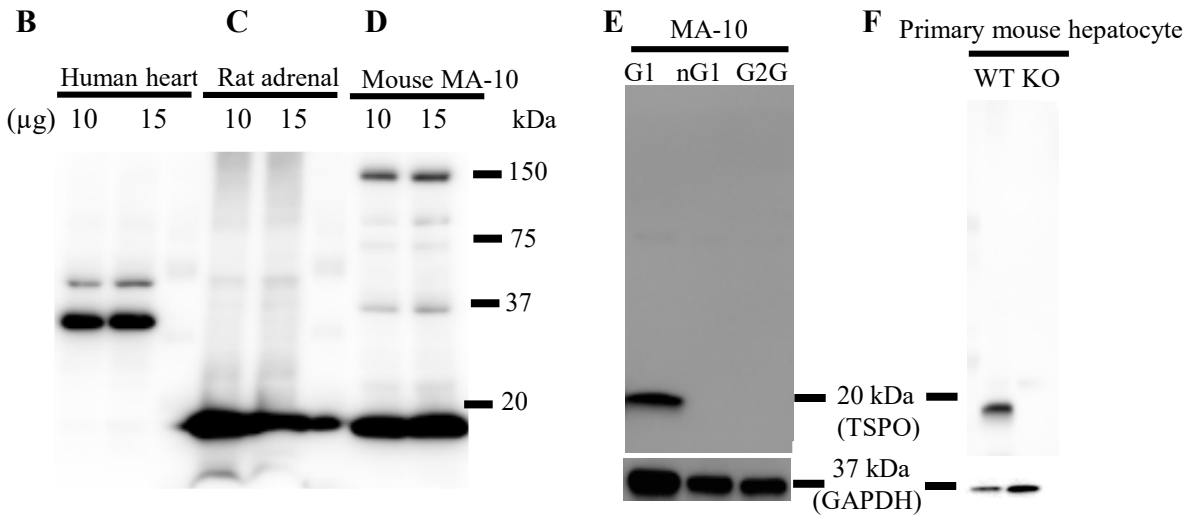

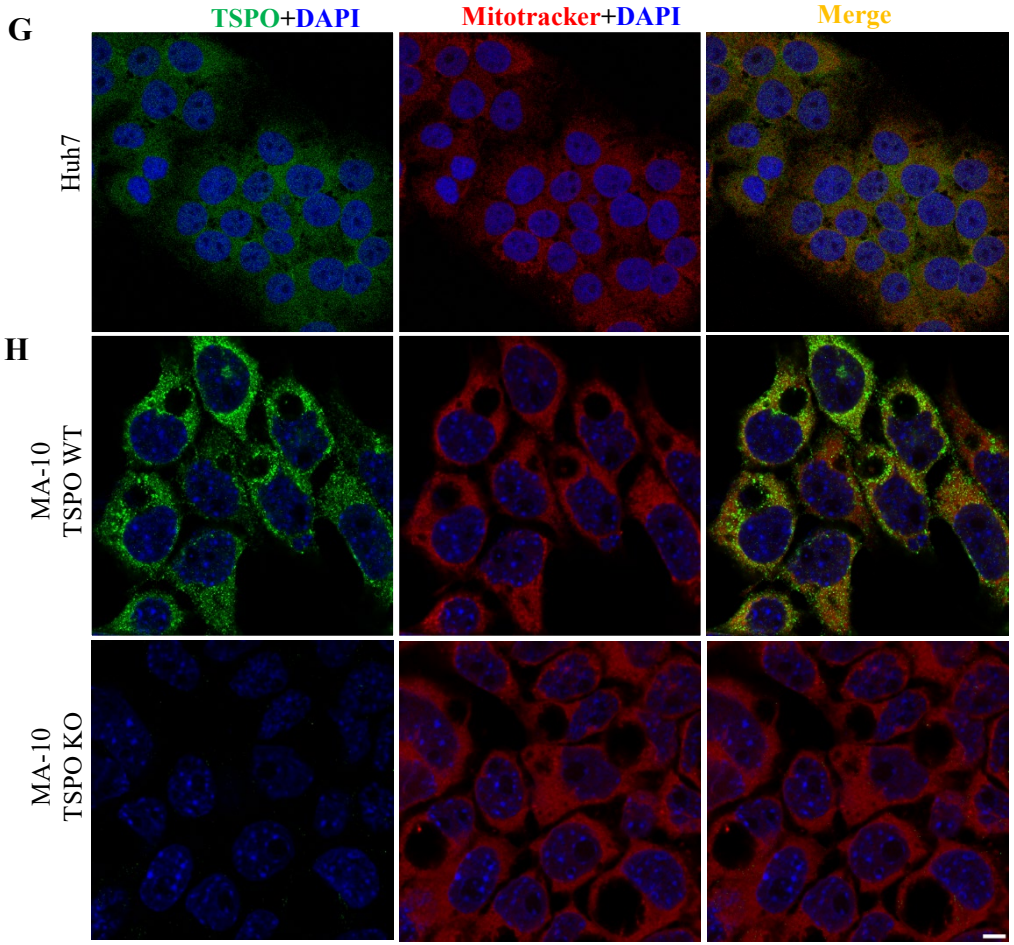

Supplemental Figure Legends

Figure S1. Related to Figure 2. The TSPO HO rats with abnormal LD accumulation displayed a steatosis phenotype. The rat liver cryosections of TSPO WT, heterozygous deletion (Het), and homozygous deletion (HO, in main text as KO) was stained with Oil Red O (red color). The results show abnormal LD (Lipid droplet) accumulation, one hallmark of steatosis, in *Tspo* HO rats compared to WT and Het. Scale, 200μm.

Figure S2. Related to Figure 2. Free cholesterol elevation in TSPO-deficient cells. (A) Dil-AcLDL uptake in Huh7 cells. Huh7 cells were treated with Dil-AcLDL (50μg/mL) (red color) for 24hrs, the cells were fixed in 4%PFA for 10min. After PBS washing 3 times, the cells nuclear was stained with DAPI. The images were captured under an inverted microscope. (a): Huh7 cells were treated with DMSO as control. (b): Huh7 cells were treated with Dil-AcLDL. Scale bar, 40μm. (B) TSPO was knocked out (KD) using different human *Tspo* siRNAs (siRNA-1, -2 and -3) in humanized mouse hepatocytes, α-Tubulin was used as the loading control. (C) Total cholesterol (TC), free cholesterol (FC) and cholesterol ester (CE) were measured in primary WT and TSPO KD (*Tspo* siRNA 2) humanized mouse hepatocytes. Data are represented as mean ± SD, *$p<0.05$, **$p<0.01$ by one-way ANOVA.

Figure S3. Related to Figure 2. Triglycerides and fatty acids distribution in WT and TSPO KO mouse liver. (A) Triglycerides (yellow) are observed both as Na^+ and K^+ cations, with similar distributions for both ions in TAG (50:2), (52:4), (52:3) and (52:2). The blue indicating blood vessels. Scale, 9mm. (B) For bile ducts, taurocholic acid was observed as an [M-H+2K] + ion. For blood vessels, heme is observed as [M+] ions. In general, the TAGs were not strongly localized with either the bile ducts or blood vessels. Bile ducts: yellow. Blood vessel: blue. Scale bar, 5mm. (C) Fatty acids (yellow) were analyzed using negative ion mode with 9-AA matrix. A few of the fatty acids were observed in WT and KO tissues, with fatty acids generally being more abundant in KO tissue. Similar to the triglycerides, the fatty acids were not localized near the blood vessels (blue), but in general were fairly evenly distributed around a liver. The plots for each of the observed fatty acids showed similar trends. Specifically, elevated levels of all the observed fatty acids were observed in the KO liver compared to WT liver. a, palmitoleic/sapienic acid; b, linoleic/linoelaidic acid; c, oleic/elaidic/vaccenic acid; d, eicosapentaenoic acid; e, arachidonic acid; f, docosahexaenoic acid. Scale, 8mm. Data represented as mean ± SD.

Figure S4. Related to Figure 3. TSPO directly interacts with ACAT2 in a manner independent of cholesterol accumulation. After co-transfection of TSPO-myc plasmid and ACAT2-Turbo-GFP plasmid into WT Huh7 cells, we validated the overexpression of ACAT2 with ACAT2 antibody (A) and TSPO with C-Myc antibody (B), respectively. After incubation of the anti-Turbo-GFP antibodies with clarified cell lysates, immunoblotting by Turbo-GFP (control, C) and C-Myc antibody, the results showed 18-20 kDa of TSPO band (D). The cells were treated with AcLDL or AcLDL+58035 and immunoprecipitated with GFP antibody, the results showed TSPO and ACAT2 interacted in a manner independent of cholesterol accumulation (C, D). QPCR of *Acta2, Lxra, Hmgcr* and *Srebp-1c* in primary WT and TSPO KO hepatocytes with DMSO, AcLDL and AcLDL+58035 treatment (E). Data are represented as mean ± SD, *$p<0.05$ by Student's t-test. HMGCR immunoblot in WT and TSPO KO primary mouse hepatocytes with DMSO, AcLDL and AcLDL+58035 treatment (F). Immunoprecipitation with ACAT2 antibody and immunoblot with ubiquitin in WT and TSPO KO mouse hepatocytes (G).

Figure S5. Related to Figure 4. Lipid droplet frequency distribution after treatment with U18666A, MβCD/CHOL, MβCD/CHOL+58035 or oleic acid in Huh7. (A) LDs distribution (size, number) in Scram and TSPO KD Huh7 cells after U18666A treatment for 24hrs. LDs were isolated, stained with nile red, imaged (left panel) and quantified (right panel). (B) LDs distribution (size, number) in Scram and TSPO KD Huh7 cells after MβCD/CHOL or MβCD/CHOL+58035 treatment for 24hrs. The LDs were isolated, stained with nile red, imaged (left panel) and quantified (right panel). CHOL: cholesterol. (C) LDs distribution (size, number) in Scram and TSPO KD Huh7 cells after treatment with BSA or oleic acid (OA) for 24hrs. The LDs were isolated, stained with nile red, imaged (left panel) and quantified (right panel). Scale, 50μm.

Figure S6. Related to Figure 5. No change of ATF6 between WT and TSPO KO. ATF6 immunoblot in WT and TSPO KO primary mouse hepatocytes with DMSO, AcLDL and AcLDL+58035 treatment.

Figure S7. Related to Figure 6. The LD size in Scram and TSPO KD Huh7 cells after treatment with AcLDL. The Scram and TSPO KD cells were treated with DMSO and AcLDL for 24hr and then observed under TEM. Compared to Scram, the LD diameters in TSPO KD cells were enlarged with AcLDL treatment. LD, red arrow; ER, blue arrow. Scale, 500 nm.

Figure S8. Related to Figure 7. MCD diet mediated transcriptome changes in reflection in TSPO KO rats. (A) The scatterplot of RNA-seq gene expression analysis between WT chow vs. WT MCD. MCD diet mediated transcript expression data farthest away from the diagonal line were selected for further analysis. (B) The selected data points from A were overlaid on the RNA-seq transcript expression data from TSPO KO rats: KO chow vs. KO MCD. Apparently, the MCD diet-related genes were affected by TSPO KO. (C) The up-regulated MCD-mediated genes from WT are overlaid on RNA-seq transcript expression data from TSPO KO rats. Some TSPO KO specific down-regulated genes are selected (in dark), accounting for 9.9 % of the total MCD diet up-regulated genes. (D) The down-regulated MCD-mediated genes from WT were overlaid on RNA-seq transcript expression data from TSPO KO rats. Some TSPO KO specific up-regulated genes are selected (in dark), accounting of 35.7% of the total up-regulated genes by MCD diet. (E) The scatterplot of RNA-seq gene expression analysis between TSPO KO chow vs. KO MCD. The MCD diet-mediated transcript expression data farthest away from the diagonal line were selected for further comparison. (F) The MCD diet-mediated gene expression from TSPO KO rats were laid over the WT rats. Both TSPO KO vs WT shared 82.2% genes that were up-regulated and 24.9% of genes that were down-regulated. (G, H) The selected genes with over 2-fold difference between KO vs WT (chow) and KO vs WT (MCD). (I, J) The selected genes with over 5-fold difference between KO vs WT (chow) and KO vs WT (MCD).

Figure S9. Related to Figure 7. The comparisons of NASH markers (*Col1a1, Acta2*) and cholesterol metabolism markers (*Cyp27a1, Cyp7a1, Fgf21* and *Tspo*) between WT chow/WT MCD and KO chow/KO MCD rats. (A) The NASH markers *Col1a1, Acta2* and cholesterol metabolism markers of *Cyp27a1, Cyp7a1,* and *Fgf21* mediated by MCD diet are up regulated in the WT MCD rats. (B) The same markers are shown in the TSPO KO rats. Remarkably, the *Fgf21* was down-regulated in TSPO KO MCD but up-regulated in KO chow. (C) *Tspo* was up regulated after MCD diet than in Chow diet. (D) *Tspo* was higher in WT-Chow than in KO-Chow. (E) *Tspo* was higher in WT-MCD than in KO-MCD.

Figure S10. Related to Figure 2. TSPO mainly expressed in the primary HSCs. Hepatocyte (HC), Kupffer cells (KC) and Hepatic stellate cells (HSC) was isolated from rat and the real-time PCR was performed. mRNA relative expression is *Tspo/Gapdh*.

Figure S11. Related to Figure 1 and 7. Characterization of the generated TSPO polyclonal antibody in rabbit. (A) Comparison of conserved peptide sequence in different species. Western blots of TSPO in (B)human heart lysate, (C) rat adrenal lysate, (D) mouse tumor Leydig cell line MA-10, and (E) mouse MA-10 (G1) and two MA-10 TSPO knockout (nG1 and G2G) cell lines, and (F) in primary hepatocytes from TSPO wild type and TSPO KO mouse. GAPDH was used as an internal control. (G) Co-staining of TSPO (green) and Mitotracker (Mit) (red) in WT human Huh7 cells. (H) Co-staining of TSPO (green) and Mit (red) in mouse TSPO WT MA-10 and TSPO KO MA-10 cells. Nuclear is stained by DAPI. Scale, 20μm.

Transparent Methods

EXPERIMENTAL MODEL AND SUBJECT DETAILS

Standard Protocol Approvals and Patient Consent

The NAFLD patient study was done in accordance with the guidelines approved by McGill University Health Centre Institutional Review Board (IRB). Prior written informed consent was obtained from all subjects who participated in the study (protocol: SDR-11-669).

Experimental Animals

TSPO KO mice were generated in our laboratory (Fan et al., 2020). *Tspo* mutant rats (Het and KO) were generated using CompoZr® knockout Zinc Finger Nuclease Technology to delete an 89-bp fragment flanking the exon 3/intron 3 junction in *Tspo* gene (Owen et al., 2017). The mice or rats were bred and maintained in accordance with protocols approved by the IACUC of the University of Southern California.

For the NAFLD model, seven-week-old male C57BL/6J mice (Jackson Labs) were allowed to acclimate housing in our facility for 2 weeks before dietary intervention. Mice were fed a diet to induce NASH with the fructose-palmitate-cholesterol diet (FPC, Tekland) incorporating 1.25% cholesterol for 20 weeks (n=12). The drinking water was supplemented with 23.1g/L of glucose and 18.9 g/L fructose (55%/45% glucose/fructose ratio). Age-matched mice maintained on chow or FPC diet incorporating 0.05% cholesterol served as normal (n=6) and steatosis (n=12), respectively.

For MCD (methionine choline deficient) diet studies, TSPO WT and KO male rats aged 12 wks old were fed either regular rat chow or an MCD diet (MP Biomedicals, #960439; n = 4) for 8 wks. The rats were divided into 4 groups (WT chow, KO chow, WT MCD and KO MCD, n=4). The body weight was recorded every week. After 2 mo, deeply anesthetized rats were decapitated and trunk blood was collected into tubes (BD Vacutainer, 367820), or into a microcontainer (BD Microtainer Blood Collection Tubes, 365965) followed by 10 min centrifugation at 1200×g. The serum was collected from BD Vacutainer for bile acid analysis, the plasma was collected from BD Microtainer Blood Collection Tubes for albumin, alanine aminotransferase (ALT), aspartate aminotransferase (AST), Alkaline Phosphatase, glucose, total bilirubin, total cholesterol, and triacylglycerol measurement (Antech Diagnostics, CA, USA). Fresh liver tissue samples from WT chow, KO chow, WT MCD and KO MCD were placed into micro-Eppendorf tubes and stored in -80^{o}C for protein and RNA analyses. The left lobe from the livers from the above 4 groups were sliced with a scalpel approximately 0.5 cm in maximal dimension and fixed in 4% phosphate-buffered paraformaldehyde for 2h.

Cell culture

Human liver Huh7 cells (originally isolated from a liver tumor from a 57-year-old Japanese male) were purchased from JCRB Cell Bank. Cells, both non-transfected and transfected (see below), were grown in DMEM (Dulbecco's modified Eagle medium) supplemented with 10% heat-inactivated fetal bovine serum (Hi-FBS) and 1% penicillin-streptomycin. Cells were kept at 37^{o}C in a humidified incubator with an atmosphere of 5% CO2.

To observe AcLDL uptake, Huh7 cells at 80% confluence were treated with Low Density Lipoprotein from Human Plasma, Acetylated, DiI complex (DiI AcLDL) (50μg/mL) for 24 hrs.,

and cells were then fixed in 4% PFA for 10 min. Cells were washed 3 times with PBS, and nuclei were stained with DAPI. The images were captured with an inverted fluorescent microscope (REVOLVE, Echo, USA). For cholesterol accumulation, stable cell lines of Scram Huh7 and TSPO KD Huh7 cells were seeded until confluence reached approximately 80% and then treated with DMSO, AcLDL (Thermo Fisher Scientific, #J65029-8+, 50 μg/mL) or AcLDL and compound 58035 (Sigma, #S9318, 10 μg/mL) for 24 hrs. For the TSPO CRAC inhibitor experiment, 80% confluence Huh7 cells were treated with DMSO, AcLDL (50 μg/mL) or AcLDL (50 μg/mL) +5-Androsten-3, 17, 19-triol (19-Atriol) (100 μM) for 24 hrs., and the cells were then collected for TC and FC measurements. For cholesterol depletion using methyl-β-cyclodextrin (MβCD), KD and Scram cells were seeded in human Lipoprotein Deficient Serum (LPDS; LP4, Sigma). After treatment for 24 hrs., cells were harvested for isolation of lipid droplets with the Lipid Droplet Isolation Kit (Cell Biolabs, Inc. MET-5011). For the accumulation of free fatty acids, KD and Scram cells were treated with either 5% bovine serum albumin (BSA; fatty acid-free, endotoxin-free; IC15240105, Sigma) or 400 μM OA (O3008, Sigma) for 24 hrs. Cells were harvested for isolation of lipid droplets with the Lipid Droplet Isolation Kit (Cell Biolabs, Inc. MET-5011). For OA treatment, KD and Scram cells were treated with either 5% bovine serum albumin (BSA; fatty acid-free, endotoxin-free) or 400 μM OA for 24 hrs.

Primary mouse hepatocytes were isolated from a 8-week-old wild type male C57BL/6 and a TSPO global knock out (KO) male mouse using a two-step collagenase perfusion protocol through the portal vein (Severgnini et al., 2012). Perfusions yielded 80% initial cell viability by trypan blue exclusion and a final 93% viability following Percoll gradient centrifugation. The hepatocytes were seeded at 1×10^6/ml in basic medium containing insulin (1 μg/ml), hydrocortisone (0.25 μM) for 4 hrs or until cells were fully attached to the collagen I (Gibco, USA) coated wells, then the medium was replaced with 10% Hi-FBS DMEM. After incubation overnight, the cells were treated as noted above for cell lines.

Primary rat hepatocytes were isolated from an 8-week-old male Sprague Dawley. The isolation is as the same as described above for mouse hepatocytes. The male rat HSCs (hepatic stellate cells) and KCs (Kupffer cells) were isolated by gradient ultracentrifugation of a non-parenchymal cell-enriched fraction following pronase-collagenase digestion of the liver by the Southern California Research Center for ALPD and Cirrhosis (Li et al., 2016; Xiong et al., 2008). Cell viability was ascertained by trypan blue dye exclusion and for both HSCs and KCs was about 95%.

Human hepatocytes were isolated from humanized liver chimeric mice (HLCM). In brief, HLCM were produced by an injection of commercially available cryopreserved primary human hepatocytes (PHH) (Lot: JFC, 1-year old, Caucasian male, BioIVT Westbury, NY) into the spleen of severe combined immunodeficiency (SCID) mice with albumin enhancer/promoter driven cDNA-urokinase type plasminogen activator (cDNA-uPA) transgene expression (Tateno et al., 2015). The use of PHH for the production of HLCM has been approved by Utilization of Human Tissue Ethical Committee of PhoenixBio Co., Ltd. (0031). After 13-27 weeks post PHH injection, HLCM with high replacement rates (>90%, estimated by blood human albumin levels which is highly correlated with histological replacement index (Sugahara et al., 2020) were subjected to human hepatocyte isolation. Human hepatocytes were isolated by a two-step collagenase perfusion method as described previously (Yamasaki et al., 2020).

See results for which cell lines or isolated cells were used in any one experiment done with the methods detailed below. The methods did not change between cell lines or isolated cells except as noted.

METHOD DETAILS

Clinical Data

This study included a total of 12 liver specimens from 12 patients undergoing liver resection for different etiologies. Following sharp resection of a small liver specimen, samples were immediately perfused with ice-cold normal saline solution. After gross examination by a pathologist, samples were released. All samples were scored by a pathologist according to the NAFLD Activity Score (NAS) (Kleiner et al., 2005): normal livers (n=3), livers with steatosis (n=3), non-alcoholic steatohepatitis (NASH) (n=3) and cirrhosis (n=3) **(Table S1)**.

Immunohistochemical (IHC) Staining of Human Samples

Formalin-fixed, paraffin-embedded (FFPE) human CRCLM resected blocks were used for this study. Serial sections 4 μm thick were cut from each FFPE block, mounted on charged glass slides (Superfrost Plus; Fisher Scientific, Waltham, MA), and baked at 65°C for 1hr prior to staining. IHC staining was performed using the Ventana BenchMark LT fully automated machine (Ventana Medical System Inc. Arizona, USA) and stained for TSPO (1:2000; Monoclonal rabbit Anti-Human PBR, Abcam cat. No ab109497) using extended antigen retrieval (CC1 buffer). Antibodies see **Table S5.**

Histopathological Analysis and Scoring of Human Samples

All human patients' slides were scanned at 40X magnification using the Aperio AT Turbo system. Images were viewed using the Aperio ImageScope ver.11.2.0.780 software program for scoring analysis and assessment of signals. The positivity was assessed with an Aperio ScanScope (Aperio Technologies Inc., Vista, CA), ImageScope software, and an optimized algorithm (positive pixel count V9, Aperio, Inc.).

Histology Slides Preparation and Picro-Sirius Red Staining of Rat MCD Fed Samples

PFA fixed liver tissues were dehydrated by sequentially increasing ethanol concentrations, cleared in xylene, and then embedded in paraffin wax. The liver collagen after MCD feeding was visualized with Picro-Sirius Red Stain Kit (American MasterTech, Pint Kit Item: KTPSRPT). Briefly, the paraffin slides were deparaffinized with xylene, rehydrated in gradient concentration of alcohol (100%, 95%, 70%, 50%) and rinsed with deionized H_2O. The slides were immersed in Picro-Sirius red stain solution for 1min following by a 0.5% acetic acid rinse. After dehydration in absolute alcohol. The slides were cleared in xylene and mounted with permanent mounting media. The images were captured with an inverted microscope (REVOLVE, Echo, USA). The collagen density was quantified using Image J software.

Generation of Stable TSPO KD Cell Line in Huh7

Huh7 cells were transfected with human PBR (TSPO) shRNA plasmid (Cat#: sc-40821-SH, Santa Cruz) or Scramble shRNA plasmid-A (Scram) (Cat#: sc-108060, Santa Cruz) using Lipofectamine 3000 Transfection Reagent (Thermo Fisher Scientific, Cat# L3000001). After 2 days of transfection, the cells were selected with puromycin (1 mg/ml) for two weeks. The cells were then

harvested and subjected to immunoblotting and confocal detection to confirm knockdown before use. The resulting cell lines were TSPO KD and Scram.

siRNA transfection

Human hepatocytes were transfected with human TSPO siRNA (Millipore Sigma, NM_000714: SASI_Hs01_00054085 for siRNA-1; SASI_Hs01_00054086 for siRNA-2 and SASI_Hs01_00054085 for siRNA-3, Millipore Sigma) and negative control siRNA (SIC001-5X1NMOL, Millipore Sigma) following the instructions of Lipofectamine™ RNAiMAX Transfection Reagent (Invitrogen, Cat# 13778150). The transfection efficiency was determined by immunoblot against rabbit TSPO antibody. After comparison, TSPO siRNA-2 was chosen for later experiments.

Matrix-assisted Laser Desorption/ionization (MALDI) Imaging Mass Spectrometry (IMS)

WT and TSPO KO mice 3 months old males were harvested, and the left liver lobe dissected and immediately placed on an aluminum boat floating on liquid nitrogen for 3-5 minutes. The frozen tissue was stored in -80°C for later use or immediately mounted onto a specimen disc using OCT as a mounting glue for cryostat sectioning (thickness 10 µm). The tissue sections were placed onto a Bruker ITO-coated slide (Bruker, Cat# # 237001). Slides were kept frozen at -80C until shipped on dry ice to Bruker Scientific LLC (Billerica, MA, USA). TC, CE, fatty acids, and triglycerides were examined in positive ion mode. The images were generated with SCiLS software.

Quantitative Real-time PCR (qPCR)

Total RNA was extracted from cells or tissues using Quick-RNA™ MiniPrep (#R1054&1055, Zymo Research, USA). Reverse-transcription was performed using a PrimeScript RT reagent kit (#RR037A, Takara, USA). qPCR was amplified with SYBR Green Real-Time PCR Master Mixes (#A25742, Thermo Fisher Scientific, USA) and performed on Real-Time PCR Instruments (CFX384, BIO-RAD, USA). The oligonucleotides used are listed in **Table S3**. The internal control is *Gapdh* or ribosomal protein *S18 (Rps18)*. The relative mRNA levels per sample were calculated by subtracting the detection limit (40 Ct) from the cycle threshold value (Ct) of each gene in the same sample to obtain the ΔCt value. Taking the log2 of −ΔCt resulted in the relative expression value of each gene for each sample expressed in arbitrary units. Each value was normalized against that of *Gapdh* or *Rps18*. The samples were run independently in triplicate.

MTT Assay

Cell viability was assessed with the MTT (3-(4,5-dimethylthiazol-2-yl)-2,5-diphenyltetrazolium bromide) colorimetric assay (Roche, #11465007001). Briefly, the cells were seeded in a 96-well plate for overnight until confluence reached approximately 90%, and the cells were then treated with AcLDL or AcLDL + 58035 for 24 hrs. Next, the MTT solution (5 mg/mL) was added to each well for 4 h at 37°C. The resulting formazan crystals were dissolved in solubilization solution and incubated overnight at 37°C. The optical density (OD) at 595nm was then read with a Multimode Plate Reader VICTOR X5 (PerkinElmer, USA). Each treatment was replicated six times.

Lipid Droplet Isolation and Quantification

The LDs were isolated from cells with the Lipid Droplet Isolation Kit (Cell Biolabs, Inc. MET-5011). In the final step, 200µl LDs from the top LD-enriched fractions in the tube (containing the floating LDs) were picked up and transferred to a fresh microcentrifuge tube. For quality control,

samples of LD-enriched fractions were subjected to western blot for the detection of Perilipin-1, 2 and 3; only the samples with no detectable GAPDH were used for further study. For the LD size-frequency distribution study, the LDs were diluted 10 times with PBS and stained with BODIPY 558/568 C12 (Thermo Fisher Scientific, D3835) for 15min in the dark. LDs were then put onto slides and observed under a fluorescence microscope on the TXRED channel (REVOLVE, VWR). Twenty images in different fields were randomly captured using a 10-x objective. The size of the LD was quantified with ImageJ software (NIH, Bethesda, MD, USA).

Nile Red Staining

Nile red staining was used to localize and quantitate intracellular lipids. Briefly, 10,000 cells/100µl were seeded either in a Corning 96-Well Black Polystyrene Microplate (Sigma, CLS3603-48EA) or on coverslips inside a petri dish filled with phenol red-free complete medium (Gibco, USA) overnight. The cells were exposed to AcLDL or AcLDL+58035 for 24 h. For fluorescence observation, cells were washed twice with PBS and fixed with 4% (wt/vol) paraformaldehyde (PFA) for 10 min. Then the fixed cells were washed twice with PBS and quenched with 50mM glycine in PBS for 10min. Intracellular neutral lipids were stained with Nile red staining solution (1:100 dilution from 10mg Nile red/10ml DMSO) for 15 min in the dark. Cell nuclei were stained with DAPI (4', 6-diamidino-2-phenylindole). All the staining procedures were performed at room temperature protecting the samples from light. Images were acquired with an inverted fluorescence microscope (REVOLVE, Echo, USA). LD size was quantified with ImageJ software.

Cholesterol Quantification

Total cholesterol and free cholesterol levels were measured with a Cholesterol Quantitation Kit (Sigma, MAK043-1KT). Briefly, 1×10^6 cells were trypsinized and washed with PBS, and 300ul of chloroform:isopropanol:IGEPAT CA-630 (7:11:0.1) was added in each 2ml microcentrifuge tube. The cells were homogenized by the TissueLyzer II (Qiagen, USA). After centrifugation, the organic phase was transferred to a new tube and dried at 50°C in a SpeedVac Concentrator (Thermo, SPD131DDA) for 30min to remove the chloroform. The dried lipids were then dissolved in Cholesterol Assay Buffer. A standard curve was prepared with cholesterol standard solution and cholesterol assay buffer. In a 96-well plate, 50 µl of samples and standards (1-5ng) were added to the reaction mixture and incubated at 37°C for 1 hr covered with aluminum foil. The absorbance was detected at 570nm with a Multimode Plate Reader VICTOR X5 (PerkinElmer, USA). Each sample was replicated four times.

Triacylglycerol (TAG) Quantification

Triglyceride quantification followed commercial kit instructions (#ab65336, Abcam) with modifications. Briefly, 10^6 cells were plated and harvested 24 hours after treatment. Cells were then resuspended and homogenized in 500 µl of 5% NP-40/ddH2O solution, followed by 5 minutes heat on a heater block and then cooled down to RT. Samples were centrifuged at 13,500 rpm for 5 mins, and 200 ul supernatant was transferred to a new tube for measurement. Standard was prepared following the instructions. Then, 50 ul of samples or standard were loaded to 96 well plates in duplicate, and 2 ul of ligase was added to each well for 20 mins incubation at RT. Finally, 50 ul of enzyme mix was added to each well of sample or standard, incubated for 1 hour at RT protected from light, and the absorbance read at 570 nm. The results were normalized to protein concentration.

Immunofluorescence Staining and Confocal Microscopy

The slides were baked at 65°C for 30 hrs prior to staining. After de-paraffinization with xylene, the slides were rehydrated with series gradient ethanol from 100%, 95%, 70%, 50% and rinsed with deionized H_2O. 0.1% Trion X-100 was used for permeabilization and 5% donkey serum in 3% BSA/PBS was used to block non-specific background. Anti-TSPO (1:400; polyclonal rabbit, generated by the Papadopoulos laboratory, see supplemental information) was incubated with the slides at 4°C overnight. The anti-Rabbit IgG (H+L) Highly Alexa Fluor 647 antibody (Cat# A-31573, Thermo Fisher Scientific) was incubated for 30 mins. DAPI was added for nuclear staining. Images were acquired with an inverted fluorescence microscope (REVOLVE, Echo, USA).

Cells were seeded onto coverslips at 200,000 cells/ml in 12-well plate. For mitochondria staining, 100 nM MitoTracker Deep Red FM (Thermo Fisher Scientific, M22426) was added to the cells. After treatment, cells were fixed in 4% PFA for 10 mins, followed by permeabilization with 0.1% Triton X-100 for 10 mins and blocking with 5% donkey serum in 3% BSA/PBS for 30 mins. The cells were then incubated with primary antibodies against TSPO or ACAT2 (See **Table S5**) at 4°C overnight. After rinsing with PBS, cells were incubated with the appropriate second antibodies (See antibodies in **Table S5**). DAPI was added for nuclear staining. Images were captured with a ZEISS LSM 880 with Airyscan confocal microscope (Carl Zeiss, Germany) using a 63× Oil objective. Identical settings were used for Scram and KD cells.

Immunoblotting and Co-immunoprecipitation (Co-IP)

The proteins were extracted with RIPA buffer (Santa Cruz Biotechnology USA, sc-24948A) containing Protease Inhibitor Tablets (Pierce, #A32963). Protein concentration was determined by BCA Protein Assay (Pierce, #23225). 10µg protein was subjected to 4-20% SDS-PAGE. After transfer to the PVDF (polyvinylidene difluoride) membrane, proteins were blocked in 5% BSA I PBS containing 0.1% Tween-20 (PBST) for 30 mins. The primary antibody was incubated with the membrane at 4°C overnight. After washing by PBST, the horseradish peroxidase-conjugated secondary antibody was added and incubated for 1 hr. After washing with PBST, the protein band was visualized by Chemiluminescent substrate for quantitative chemiluminescent western blots (Radiance Plus, #AC2103, Azure) on an Azure Biosystem (Azure c600) (Primary and secondary antibodies were listed in **Table S4**). GAPDH antibody or β-actin antibody was used as an internal control. The protein band was quantified by densitometry using Image J software.

For the Co-IP assay, PBR Human Tagged ORF Clone (TSPO; NM_000714; RC220107, Origene) and Human Tagged ORF Clone ACAT2 (NM_005891; RG201821, Origene) was transfected into WT Huh7 cells. The protein was extracted from the transfected cells with Lysis/Equilibration Buffer, the interaction between TSPO-Myc and ACAT2-TuboGFP protein was performed according to the instructions for Capturem™ IP & Co-IP Kit (Takara, #635721).

For the ACAT2 antibody IP assay, WT and TSPO KO mouse hepatocytes were isolated as above. After 3 hrs culture, the medium was replaced with DMEM supplemented with 10% Hi-FBS and 1% penicillin-streptomycin, and the cells were cultured for 24 hrs. Then the cells were harvested, and the cell pellets lysed according to the instruction of Immunoprecipitation kit (Abcam, Cat# ab206996). The solubilized protein was immunoprecipitated with anti-rabbit ACAT2 (Cell signaling, Cat# 13294). For the immunoblot, after the protein separation by SDS-PAGE, the PVDF

membrane was probed with Ubiquitin monoclonal antibody (Ubi-1, # 13-1600, Thermo Fisher Scientific).

Duolink Proximity Ligation Assay (PLA)

Duolink In Situ Red Starter Kit (DUO92105) was purchased by Sigma-Aldrich. The assay was run per kit instructions. Briefly, Huh7 cells were seeded on a coverslip overnight. After 4% PFA fixation, the cells were covered with blocking solution. The cells were then incubated with anti-goat TSPO (LifeSpan, Cat# LS-B5755-50) and anti-rabbit ACAT2 (Cell signaling, Cat# 13294) overnight. The Duolink In Situ PLA probe anti-rabbit PLUS and Duolink In Situ PLA probe anti-goat Minus was incubated with cells for 1hr at 37°C. The ligation and amplification proceeded per the manufacturer's instructions. Coverslips were mounted with Duolink In Situ Mounting Media with DAPI. The images were captured under a ZEISS LSM 880 with Airyscan confocal microscope (Carl Zeiss, Germany) using a 63× Oil objective.

Transmission Electronic Microscopy (TEM)

1×10^6 cells were harvested and fixed in 1/2 strength Karnovsky solution containing 2.5% glutaraldehyde (EM grade, Sigma) and 2% paraformaldehyde in PBS overnight at 4°C. The cell pellet was rinsed in 0.1M cacodylate buffer and post-fixed in 2% aqueous OsO_4/0.2M cacodylate buffer for 2 hours at 4°C, followed by rinsing several times with 0.1M cacodylate buffer. The cells were then EM-block stained with statured uranyl acetate at 4°C overnight. After rinsing with 0.1M sodium acetate buffer, the cells were dehydrated through a gradient series of: 70% EtOH (ethanol), 15 min; 90% EtOH, 15 mins; 100% EtOH, 2×15 mins; propylene oxide (PO)/EtOH (1:1), 15 mins; PO/ETOH (2:1), 15 mins; and PO, 2×15 mins. Cells were then infiltrated with Epon resin/PO (1:1) overnight. After that, the cells were placed into Epon resin/PO resin (2:1) for 8 hrs, followed by vacuum polymerization in 100% Epon resin overnight. Cells were then embedded in fresh Epon resin at 60 °C for 24 hrs and subjected to ultra-thin sectioning (~70nm). The thin sections were transferred to 200 mesh copper grids and stained with 2% uranyl acetate for 30 mins and 2.66% lead citrate (pH 12) for 10 mins. The images were acquired under transmission electron microscopy (JEM-2100 Electron Microscope, Japan) at the Doheny Eye Institute (Los Angeles, USA).

RNA-seq Library Preparation and Sequencing

Libraries for RNA-Seq were prepared with Kapa Stranded mRNA. The workflow consisted of mRNA enrichment, cDNA generation, end repair to generate blunt ends, A-tailing, adaptor ligation, and PCR amplification. Different adaptors were used for multiplexing samples in one lane. The RNA sequence data was generated on an HiSeq3000 for a single-read 50bp read run. A data quality check was done on an Illumina SAV. Demultiplexing was performed with Illumina Bcl2fastq2 v 2.17 program. RNA-seq data were deposited in the Gene Expression Omnibus under accession number GSE138666 (https://www.ncbi.nlm.nih.gov/geo/query/acc.cgi?acc=GSE138666).

RNA-seq Data Analysis

All analyses were performed in Partek® Flow® software, version 8. For alignment, unaligned sequenced reads were trimmed from both ends to a fixed-length dependent on the positional base at which the PHRED quality score fell below 20. A minimum read length filter retaining reads greater than 25 bases in length were used. Trimmed reads were aligned to the rat genome assembly, rn6 using the STAR (version 2.6.1d) aligner. A seed mismatch limit of 1 was applied. Raw read

counts were obtained by quantitating aligned reads to rn6 (Ensembl Transcripts release 96), using a modified version of the expectation-maximization algorithm. For normalization, reads with raw counts > 10 were normalized using the Upper Quartile (UQ) normalization method. An offset of 1.0 was added to all normalized read counts. Principle components analysis (PCA) was performed to assess the overall variability in the gene dataset, in which log transformation with a log base of 2 and a log cutoff of 1.0 was applied to all normalized read counts.

For differential expression analysis, normalized read counts for each gene were statistically modeled using differential gene expression algorithm (GSA) that uses the Akaike Information Criterion corrected (AICc). Comparisons were performed with KO MCD versus WT MCD, and KO CHOW versus WT CHOW, respectively. An expression filter based on the cutoff of absolute fold change > 1.2 and *P*-value < 0.05 was applied to select the differential expressed (DE) genes. Hierarchical cluster analysis was performed on the subset of DE genes that were normalized by standardizing the algorithm applied across genes. The analysis was run with Pearson Correlation distance measure and average linkage clustering option.

QUANTIFICATION AND STATISTICAL ANALYSIS

Statistical Analysis

Statistical analysis was performed with GraphPad Prism 8.4.3 (Graph Pad Software, USA). Data were presented as the means ± standard deviation (SD). Statistical significance of differences was determined using an independent t-test between two groups and significant differences more than two groups were evaluated by one-way ANOVA with Tukey-Kramer as post hoc test. $p < 0.05$ was considered statistically significant.

Key Resources Table for this study

REAGENT or RESOURCE	SOURCE	IDENTIFIER
Antibodies		
Monoclonal rabbit Anti-Human PBR (TSPO)	Abcam	Cat# ab109497; RRID: AB_10862345
Polyclonal rabbit Anti-Human FXR (NR1H4)	Abclonal	Cat# A12788; RRID: AB_2759628
Monoclonal rabbit Anti-Human ACAT2	Cell Signaling	Cat# 13294; RRID: AB_2798172
Monoclonal mouse Anti-Human Cyp7a1(clone 15B9.1)	Millipore Sigma	Cat# MABD42; RRID: AB_2756360
Polyclonal rabbit Anti-Human LC3B	Millipore Sigma	Cat# L7543; RRID: AB_796155
Polyclonal rabbit Anti-Human CYP27A1	Proteintech	Cat# 14739-1-AP; RRID: AB_2089276
Polyclonal rabbit Anti-Mouse TSPO	ProSci Inc	In this paper
Biological samples		
Human NAFLD samples	Research Institute of the McGill University Health Center, Montreal, Quebec, H4A 3J1, Canada. Department of Surgery, McGill University, Montreal, Quebec, H3G 1A4, Canada	In this paper
Healthy Human heart lysate	ProSci, Inc. CA, USA	Cat. No. 1470
Healthy Rat adrenal lysate	ProSci, Inc. CA, USA	Cat. No. 1470
Primary human hepatocytes	BioIVT Westbury, NY	Lot: JFC
Primary rat hepatic stellate cells (From Sprague Dawley)	Southern California Research Center for ALPD and Cirrhosis, Los Angeles, CA 90089, USA	https://keck.usc.edu/alpd-and-cirrhosis-research-center/

Primary rat hepatocytes (From Sprague Dawley)	Southern California Research Center for ALPD and Cirrhosis, Los Angeles, CA 90089, USA	https://keck.usc.edu/alpd-and-cirrhosis-research-center/
Primary ra Kupffer cells (From Sprague Dawley)	Southern California Research Center for ALPD and Cirrhosis, Los Angeles, CA 90089, USA	https://keck.usc.edu/alpd-and-cirrhosis-research-center/
Chemicals, peptides, and recombinant proteins		
U18666A	Calbiochem	Cat# 662015
Lipoprotein deficient serum from fetal calf	Kalen Biomedical, LLC	Cat# 880100-5
Goat-anti-rabbit HRP	Li-Cor	Cat# 926-80011
DAPI (4', 6-diamidino-2-phenylindole)	Life technologies	Cat# P36931
5-Androsten-3,17,19-triol	Mcule, Inc. CA, USA	Quotation reference I-10729
TSPO peptide	ProSci Inc	CWRDNSGRRGGSRLAE
58035	Sigma Aldrich	Cat#S9318
Bovine Serum Albumin (BSA), ≥98%, Fatty Acid-free, MP Biomedicals	Sigma Aldrich	Cat# IC15240105
Cholesterol–methyl-β-cyclodextrin	Sigma Aldrich	Cat# C4951-30MG
Chloroform	Sigma Aldrich	Cat# C2432
Collagenase, Type I	Sigma Aldrich	Cat# C0130
Ethanol	Sigma Aldrich	Cat# EX0276-1
Hydrocortisone	Sigma Aldrich	Cat# H0888
IGEPAL	Sigma Aldrich	Cat# 18896
Nile red	Sigma Aldrich	Cat# 19123
Oleic Acid-Albumin from bovine serum	Sigma Aldrich	Cat# O3008-5ML
Percoll	Sigma Aldrich	Cat# P4937
Tween® 20	Sigma Aldrich	Cat# 8221840500

BODIPY 558/568 C12	Thermo Fisher Scientific	Cat# D3835
Collagen I rat protein	Thermo Fisher Scientific	Cat# A1048301
Cocktail proteinase inhibitor	Thermo Fisher Scientific	Cat# 78430
DMEM, high glucose	Thermo Fisher Scientific	Cat# 11965118
Insulin	Thermo Fisher Scientific	Cat# 2585014
Low Density Lipoprotein from Human Plasma, Acetylated (AcLDL)	Thermo Fisher Scientific	Cat# L35354
Low Density Lipoprotein from Human Plasma, Acetylated, DiI complex (DiI AcLDL)	Thermo Fisher Scientific	Cat# L3484-200ul
NP-40 (Nonidet P-40) Surfact-Amps™ Detergent Solution	Thermo Fisher Scientific	Cat# PI85125
Pierce™ Protein A Plus Agarose	Thermo Fisher Scientific	Cat# 22811
Puromycin Dihydrochloride	Thermo Fisher Scientific	Cat# A1113803
Dimethyl sulfoxide (DMSO)	VWR	Cat# 80058-040
Isopropanol	VWR	Cat# BDH133
Critical commercial assays		
Immunoprecipitation kit	Abcam	Cat# ab206996
Triglyceride Assay Kit - Quantification	Abcam	Cat#: ab65336
Picro-Sirius Red Stain Kit	American MasterTech	Pint Kit Item: KTPSRPT
Matrix-assisted laser desorption/ionization (MALDI) imaging mass spectrometry (IMS)	BRUKER	N/A
Lipid Droplet Isolation Kit	Cell Biolabs, Inc.	Cat# MET-5011
Lipofectamine™ RNAiMAX Transfection Reagent	Invitrogen	Cat# 13778150
HPLC	ProSci Inc	N/A
MTT	Sigma Aldrich	Cat#11465007001
Cholesterol Quantification kit	Sigma Aldrich	Cat#MAK043-1KT

Duolink In Situ Red Starter Kit	Sigma Aldrich	Cat# DUO92105
PrimeScript RT reagent kit	TAKARA	Cat# RR037A
SYBR Green Real-Time PCR Master	Thermo Fisher Scientific	Cat# A25742
Lipofectamine™ 3000 Transfection Reagent	Thermo Fisher Scientific	Cat# L3000001
Quick-RNA™ MiniPrep	Zymo Research	Cat# R1054 & R1055
Deposited data		
Raw and analyzed data	This paper	GEO: GSE127915
Experimental models: cell lines		
Huh7 cell line	JCRB Cell Bank	Cat# 0403
MA-10 cells	Fan et al., 2018	In this paper
Experimental models: organisms/strains		
Rat Sprague Dawley: TSPO heterozygous (Het)	David R. Owen., 2017	Biochemical Journal 474, 3985-3999.
Rat Sprague Dawley: TSPO homozygous (HO, in main text as KO)	David R. Owen., 2017	Biochemical Journal 474, 3985-3999.
Mouse C57BL6/J	Wang, X, 2016	Cell Metab 24, 848-862.
Mouse C57BL/6J mouse: TSPO KO	Fan, Jinjiang, 2020	J Endocr Soc 4, bvaa001.
Oligonucleotides		
Human TSPO siRNA: SASI_Hs01_00054085	Millipore Sigma	NM_000714
Human TSPO siRNA: SASI_Hs01_00054086	Millipore Sigma	NM_000714
Human TSPO siRNA: SASI_Hs01_00054085	Millipore Sigma	NM_000714
negative control siRNA	Millipore Sigma	SIC001-5X1NMOL
Recombinant DNA		
PBR shRNA Plasmid (h)	Santa Cruz	Cat#: sc-40821-SH
Control shRNA Plasmid-A	Santa Cruz	Cat#: sc-108060
Software and algorithms		
Photoshop CS6	Adobe	Adobe Photoshop Version: 19.0 20170929.r.165 2017/09/29: 1138933 x64

SCiLS	Bruker	https://www.bruker.com/en/products-and-solutions/mass-spectrometry/ms-software/scils-lab.html
Zen lite	Carl Zeiss Microscopy, LLC	https://www.zeiss.com/microscopy/us/home.html
GraphPad Prism 7	GraphPad Software	http://www.graphpad.com
Aperio ImageScope software	Leica Biosystems	https://www.leicabiosystems.com/digital-pathology/manage/aperio-imagescope/
Primer-Blast	NCBI	https://www.ncbi.nlm.nih.gov/tools/primer-blast/index.cgi?LINK_LOC=BlastHome
ImageJ Software	NIH	https://imagej.nih.gov/ij/
Partek Flow	Partek Flow	https://libguides.usc.edu/healthsciences/PartekFlow
Ingenuity Pathway Analysis 2019	Qiagen	https://www.qiagenbioinformatics.com/products/ingenuity-pathway-analysis/
Other		
Chow Diet, 18% Calories from Fat	Harlan Teklad	# 2018
MCD diet	MP Biomedicals	#960439
Picro-Sirius Red Pint Stain Kit/Ea	American MasterTech	Cat# KTPSRPT
MitoTracker™ Deep Red FM	Thermo Fisher Scientific	Cat# M22426
Pierce™ IP Lysis Buffer	Thermo Fisher Scientific	Cat# 87787

Table S1. NAFLD activity score (NAS) for the patient liver samples. Related to main Figures 1.

								NAS staging								
Sample	**Sex**	**Age**	**BMI**	**Diabetic**	**Smoking**	**Type of Procedure**	**Diagnosis**	**Steatosis**	**Lobular Inflammation**	**Hepatocyte Ballooning**	**Fibrosis score**	**% Micro steatosis**	**% Macro steatosis**	**% Total steatosis**	**NAS**	**Grading**
1	Female	52	21	No	No	Resection	Biliary cystadenoma	0	0	1	1A	0	0	0	2	Normal (Low)
2	Female	51	20	Yes	No	Resection	CRCLM	0	1	0	1A	0	0	0	2	Normal (Low)
3	Male	67	20	No	Yes	Resection	CRCLM	0	1	0	1A	1	3	4	2	Normal (Low)
4	Male	64	24	No	No	Resection	CRCLM	2	1	0	1A	15	30	45	4	Steatosis (NAFLD)
5	Male	52	25	No	No	Resection	CRCLM	2	1	1	1A	10	40	50	5	Steatosis (NAFLD)
6	Female	78	19.6	No	No	Resection	CRCLM	0	1	1	1A	0.5	0.5	1	3	Steatosis (NAFLD)
7	Female	65	30	Yes	No	Resection	CRCLM	2	2	1	1A	10	30	40	6	NASH
8	Male	67	20	No	No	Resection	Net carcinoid tumor	2	3	2	1C	10	50	60	8	NASH
9	Female	72	25	No	No	Resection	CRCLM	1	2	1	2	1	9	10	6	NASH
10	Female	65	25	No	No	Resection	Benign	0	3	1	3	0	0	0	7	Cirrhosis
11	Male	75	28	Yes	No	Resection	Benign	0	3	1 or 2	3	1	3	4	7	Cirrhosis
12	Male	70	18	No	No	Resection	Klatskin tumor /Cholangiocarcinoma	0	3	2	3	0	0	0	8	Cirrhosis

Note: BMI, body mass index; CRCLM: colorectal cancer liver metastases

Table S2. Ingenuity Pathway Analysis of the genes involved in the liver diseases and functions. Related to main Figures 7.

Categories	**Diseases or Functions Annotation**	**p-value**	**Molecules**
Liver Proliferation	Proliferation of liver cells	0.00495	BMP7, IFT88, LGALS1, PIK3R1, SLC20A1, SOCS3
Liver Proliferation	Proliferation of hepatocytes	0.0347	BMP7, IFT88, SLC20A1, SOCS3
Liver Proliferation	Proliferation of oval cells	0.0892	IFT88
Liver Fibrosis, Liver Proliferation	Proliferation of hepatic stellate cells	0.303	LGALS1
Categories	**Diseases or Functions Annotation**	**p-value**	**Molecules**
Glutathione Depletion In Liver	Conjugation of glutathione	0.00772	GSTA5, GSTM1
Categories	**Diseases or Functions Annotation**	**p-value**	**Molecules**
Liver Damage	Histopathological change of liver	0.0328	DLL4
Liver Damage	Liver Damage	0.26	ADM, DLL4, TM4SF4, TSPO
Liver Damage	Hepatic injury	0.331	ADM, TM4SF4, TSPO
Categories	**Diseases or Functions Annotation**	**p-value**	**Molecules**
Biliary Hyperplasia	Hyperplasia of bile duct cells	0.00665	IFT88
Categories	**Diseases or Functions Annotation**	**p-value**	**Molecules**
Liver Cirrhosis	Cirrhosis	0.00712	CD180, CYP3A5, GCLM, GUCY1A1, IL12RB2, SSTR3, TSPO
Liver Cirrhosis	Cirrhosis of liver	0.0794	CD180, CYP3A5, GCLM, IL12RB2
Liver Cirrhosis	Compensated cirrhosis	0.0831	CYP3A5
Liver Cirrhosis	Primary biliary cirrhosis	0.145	CD180, IL12RB2
Categories	**Diseases or Functions Annotation**	**p-value**	**Molecules**
Liver Fibrosis	Fibrosis of liver portal space	0.0133	IFT88
Liver Fibrosis	Fibrosis of liver	0.0276	BMP7, IFT88, SIRT6, SOCS3
Liver Fibrosis	Migration of hepatic stellate cells	0.142	LGALS1
Liver Fibrosis, Liver Proliferation	Proliferation of hepatic stellate cells	0.303	LGALS1
Categories	**Diseases or Functions Annotation**	**p-value**	**Molecules**
Liver Inflammation/Hepatitis	Chronic inflammation of liver	0.0133	SIRT6
Liver Inflammation/Hepatitis	Infection by Hepatitis C virus genotype 1	0.0831	CYP3A5
Liver Inflammation/Hepatitis	Experimental hepatitis	0.119	SOCS3
Liver Inflammation/Hepatitis	Inflammation of liver	0.192	CYP3A5, IL12RB2, SIRT6, SOCS3, TSPO
Liver Inflammation/Hepatitis	Infection by hepatitis B virus	0.422	CYP3A5
Categories	**Diseases or Functions Annotation**	**p-value**	**Molecules**
Hepatocellular carcinoma, Liver Hyperplasia/Hyperproliferation	Metastasis of hepatocellular carcinoma	0.0198	PIK3R1
Liver Hyperplasia/Hyperproliferation	Early stage liver cancer	0.0263	SIRT6
Hepatocellular carcinoma, Liver Hyperplasia/Hyperproliferation	Development of hepatocellular carcinoma	0.0363	MGMT, PIK3R1, SOCS3
Liver Hyperplasia/Hyperproliferation	Relapsed hepatosplenic T-cell lymphoma	0.0393	POLE
Liver Hyperplasia/Hyperproliferation	Refractory hepatosplenic T-cell lymphoma	0.0393	POLE
Liver Hyperplasia/Hyperproliferation	Resectable liver cholangiocarcinoma	0.0393	POLE
Liver Hyperplasia/Hyperproliferation	Advanced liver tumor	0.0792	POLE, SSTR3
Liver Hyperplasia/Hyperproliferation	Unresectable liver cholangiocarcinoma	0.0831	POLE
Liver Hyperplasia/Hyperproliferation	Hyperplasia of liver	0.107	IFT88
Hepatocellular carcinoma, Liver Hyperplasia/Hyperproliferation	Hepatocellular carcinoma	0.133	ADCY2, AOX1, BMP7, DUSP11, ETS1, ID1, MGMT, PIK3R1, POLE, SCIMP, SOCS3, SSTR3
Liver Hyperplasia/Hyperproliferation	Locally advanced liver cholangiocarcinoma	0.148	POLE

Liver Hyperplasia/Hyperproliferation	Proliferation of liver cancer cells	0.165	SOCS3
Liver Hyperplasia/Hyperproliferation	Metastatic liver cholangiocarcinoma	0.171	POLE
Hepatocellular carcinoma, Liver Hyperplasia/Hyperproliferation	Advanced hepatocellular carcinoma	0.229	SSTR3
Hepatocellular carcinoma, Liver Hyperplasia/Hyperproliferation	Childhood type hepatocellular carcinoma	0.234	POLE
Liver Hyperplasia/Hyperproliferation	Hepatoblastoma	0.289	POLE
Liver Hyperplasia/Hyperproliferation	Liver tumor	0.337	AASS, ADCY2, AMOT, AOX1, APBA2, ARHGAP32, ARHGEF7, ATXN2, BMP7, CYP3A5, DACT2, DDIT4, DTX4, DUSP11, ETS1, GNAI1, GREB1L, GSTA5, GSTM1, HIST1H3G, ID1, IFT88, KCNJ5, KLF10, LSAMP, MCM4, MEX3B, MGMT, NAV2, NKIRAS1, PARP8, PHOSPHO2, PIK3R1, PLXND1, POLE, PRLR, RCSD1, REEP1, RPL37, RXRG, SCIMP, SEPHS2, SGPL1, SIRT6, SLC25A15, SLC39A4, SOCS3, SSTR3, TMEM167B, TMEM56, UBXN2A, WDR62, ZNF48, ZNHIT2
Liver Hyperplasia/Hyperproliferation	Liver cancer	0.374	AASS, ADCY2, AMOT, AOX1, APBA2, ARHGEF7, ATXN2, BMP7, CYP3A5, DACT2, DDIT4, DTX4, DUSP11, ETS1, GNAI1, GREB1L, GSTA5, GSTM1, HIST1H3G, ID1, KLF10, LSAMP, MCM4, MEX3B, MGMT, NAV2, PHOSPHO2, PIK3R1, PLXND1, POLE, RCSD1, REEP1, RPL37, RXRG, SCIMP, SEPHS2, SGPL1, SIRT6, SLC39A4, SOCS3, SSTR3, TMEM167B, UBXN2A, WDR62, ZNF48, ZNHIT2
Liver Hyperplasia/Hyperproliferation	Liver carcinoma	0.402	AASS, ADCY2, AMOT, AOX1, APBA2, ARHGEF7, ATXN2, BMP7, CYP3A5, DACT2, DDIT4, DTX4, DUSP11, ETS1, GNAI1, GREB1L, GSTA5, HIST1H3G, ID1, KLF10, LSAMP, MCM4, MEX3B, MGMT, NAV2, PHOSPHO2, PIK3R1, PLXND1, POLE, RCSD1, REEP1, RPL37, RXRG, SCIMP, SEPHS2, SGPL1, SLC39A4, SOCS3, SSTR3, TMEM167B, UBXN2A, WDR62, ZNF48, ZNHIT2

Categories	**Diseases or Functions Annotation**	**p-value**	**Molecules**
Hepatocellular Peroxisome Proliferation	Formation of peroxisome membrane	0.0263	PEX11A

Table S3. Primers sequences used in the study. Related to main Figures 1, 4, 7.

SPECIES	GENE	FORWARD 5' ⟶ 3'	REVERSE 5' ⟶ 3'
Mus musculus	*Acat2*	GCGAACGCATCAGGAATGAA	TAGCTATTGCCGCAGACACC
	Dgat2	CATCACCACCGTCGTGGG	CTCCCAGGAGCTGGCAC
	Fasn	TCCGAGACCTCGCAGGTATTA	CTGTCGTGTCAGTAGCCGAGT
	Gapdh	GTTGTCTCCTGCGACTTCA	GGTGGTCCAGGGTTTCTTA
	Hmgcr	GCGTGGGATCCAAGGACTG	GCTCAGCACGTCCTCTTCAA
	LXRa	CGACAGTTTTGGTAGAGGGACA	CGCTTTTGTGGACGAAGCTC
	Plin1	CTGTCTGAGACTGAGGTGGC	TTCTCCTGCTCAGGGAGGTC
	Plin2	GCTCTCCTGTTAGGCGTCTC	TTGGCCACTCTCATCACCAC
	Ppara	GTGCAGCCTCAGCCAAGTT	TGGGGAGAGAGGACAGATGG
	Rps18	GTTGGTGGAGCGATTTGTCTGGTT	TATTGCTCAATCTCGGGTGGCTGA
	Scd1	CCCTCCGGAAATGAACGAGAG	AAAATCCCGAAGAGGCAGGTG
	Srebp-1c	GGGGCCTGACAGGTGAAATC	TGAGCTGGAGCATGTCTTCAAA
	Tspo	TAGCTTGCAGAAACCCTCTTGGCA	TGTGAAACCTCCCAGCTCTTTCCA
Rattus norvegicus	*Gapdh*	CCATTCTTCCACCTTTGATGCT	TGTTGCTGTAGCCATATTCATTGT
	F4/80	TGTCCAGCTTATGCCACCTG	TGGGCCCTGAAAGTTGGTTT
	Fgf21	ACCGCAGTCCAGAAAGTCTC	TGCAGGCCTCAGGATCAAAG
	Fxr	ATGCTGAAGCTTATGCCGGA	AAGATCCTTGGATTGCTTTGGG
	Lgals1	TACACTTCAACCCCCGCTTC	TGATGCACACCTCCGTGATG
	Rps18	ATAGCCAGGTTCTGGCCAAC	TTGGACACACCCACAGTACG
	Slc20a1	CATCCTCCGTAAGGCAGATCC	GAAAACTGCACATCCCACCG
	Tnfa	ATGGGCTCCCTCTCATCAGT	GCTTGGTGGTTTGCTACGAC
	Tspo	AGAGCATACTCTTGCCGTCG	ACTCCTAAAGGGGTTGCAGG

Table S4. List of antibodies used in western blotting. Related to main Figures 2-7.

PRIMARY ANTIBODIES	SUPPLIER	REFERENCE	DILUTION
GRP-78	Abcam	Cat# ab21685; RRID: AB_2119834	1:1000
HMGCR	Abcam	Cat# ab174830; RRID: AB_2749818	1:1000
Oxidative Stress Defense (Catalase, SOD1, TRX, smooth muscle Actin)	Abcam	Cat# ab179843; RRID: AB_2716714	1:250
PPAR alpha	Abcam	Cat# ab24509; RRID: AB_448110	1:1000
FXR	Abclonal	Cat# A12788; RRID: AB_2759628	1:1000
PLIN2	Abclonal	Cat# A6276; RRID: AB_2766881	1:1000
PERK	Cell signaling	Cat# 3192; RRID: AB_2095847	1:1000
IRE1α	Cell signaling	Cat# 3294; RRID: AB_823545	1:1000
ACAT2	Cell signaling	Cat# 13294; RRID: AB_2798172	1:1000
LAMP1	Cell signaling	Cat# 9091; RRID: AB_2687579	1:1000
ATF-4 (D4B8)	Cell signaling	Cat# 11815; RRID: AB_2616025	1:1000
α-Smooth Muscle Actin	Cell Signaling	Cat# 14968; RRID: AB_2798667	1:1000
ATG12 (D88H11)	Cell signaling	Cat# 4180; RRID: AB_1903898	1:1000

β-ACTIN	Cell signaling	Cat# 4970; RRID: AB_2223172	1:2000
CHOP (D46F1)	Cell signaling	Cat# 5554; RRID: AB_10694399	1:1000
GAPDH	Cell signaling	Cat# 2118; RRID: AB_561053	1:2000
MYC-Tag	Cell signaling	Cat# 2278; RRID: AB_490778	1:1000
CYP7A1	Millipore	Cat# MABD42; RRID: AB_2756360	1:1000
TSPO	ProSci Inc	Generated by Dr. Papadopoulos lab, see supplemental information	1:1000
Lamp2	Proteintech	Cat# 10397-1-AP; RRID: AB_2134630	1:1000
ACOX1	Proteintech	Cat# 10957-1-AP; RRID: AB_2221670	1:1000
TNF Alpha	Proteintech	Cat# 17590-1-AP; RRID: AB_2271853	1:1000
CYP27A1	Proteintech	Cat# 14739-1-AP; RRID: AB_2089276	1:1000
α-Tubulin	Sigma-Aldrich	Cat# T9026; RRID: AB_477593	1:10000
LC3B	Sigma-Aldrich	Cat# L7543; RRID: AB_796155	1:2000
CEH	Thermo Fisher Scientific	Cat# PA5-50285; RRID: AB_2635738	1:1000
CHOP	Thermo Fisher Scientific	Cat# MA1-250; RRID: AB_2292611	1:1000
TurboGFP	Thermo Fisher Scientific	Cat# PA5-22688; RRID: AB_2540616	1:1000
Ubiquitin	Thermo Fisher Scientific	Cat# 13-1600; RRID: AB_2533002	1:1000
ATF6	Novus Biological	Cat# NBP1-40256; RRID: AB_2058774	1:1000
SECONDARY ANTIBODIES	**SUPPLIER**	**REFERENCE**	**DILUTION**
Anti-Mouse IgG H&L (HRP)	Abcam	Cat# ab6728; RRID: AB_955440	1:1000
Anti-Rabbit HRP	Li-Cor	Cat# 926-80011; RRID: AB_2721264	1:10000

Table S5. List of antibodies used in immunohistochemistry and immunofluorescence.
Related to main Figures 1, 3 and 5.

PRIMARY ANTIBODIES	**SUPPLIER**	**REFERENCE**	**DILUTION**
TSPO	Abcam	Cat# ab109497; RRID: AB_10862345	1:2000
ACAT2	Cell signaling	Cat# 13294; RRID: AB_2798172	1:400
TSPO	LifeSpan	Cat# LS-B5755-50; RRID: AB_10914795	1:400
CHOP	Thermo Fisher Scientific	Cat# MA1-250; RRID: AB_2292611	1:400
TSPO	ProSci Inc	Generated by Dr. Papadopoulos lab	1:1000
SECONDARY ANTIBODIES	**SUPPLIER**	**REFERENCE**	**DILUTION**
Anti-Rabbit IgG (H+L) Highly Alexa Fluor 488	Thermo Fisher Scientific	Cat# A-21206; RRID: AB_2535792	1:400
Anti-Rabbit IgG (H+L) Highly Alexa Fluor 647	Thermo Fisher Scientific	Cat# A-31573; RRID: AB_2536183	1:400
Anti-Rabbit IgG (H+L) Highly Alexa Fluor 647	Thermo Fisher Scientific	Cat# A-31573; RRID: AB_2536183	1:400

Anti-Rabbit IgG (H+L) Highly Alexa Fluor 647	Thermo Fisher Scientific	Cat# A-31573; RRID: AB_2536183	1:400

Table S6. ELISA results for affinity purification. Related to main Figures 1, 7.

Dilutions	Serum before purification (OD450)	Immunodepleted (flow-through) after purification (OD450)	Purified Antibody at 1.0 mg/ml (OD450)
1:1,000	2.225	0.349	2.856
1:5,000	0.706	0.111	1.857
1:25,000	0.22	Not tested	0.694
1:125,000	0.092	Not tested	0.22
1:625,000	0.063	Not tested	0.105

Abbreviations: ELISA, enzyme-linked immunosorbent assay

ADDITIONAL RESOURCES

Generation and Characterization of TSPO Polyclonal Antibody

To date, there is no commercial TSPO antibody available for the protein detection in across human, mouse and/or rat species. Therefore, we attempted to generate a TSPO antibody applicable to human, mouse and rat. After comparison of all the peptide sequences from manufacturers and the literature (Hatori et al., 2012; Ji et al., 2008), we picked the peptide sequence of WRDNSGRRGGSRLAE (**Fig. S11A**) for the synthesis and performed immunogen administration into rabbits (ProSci. Inc. CA. USA). The immunoaffinity purification was performed through a chromatography column prepared by cross-linking of the synthesized TSPO peptide (CWRDNSGRRGGSRLAE) with cysteine to a CNBr-activated Sepharose 4B gel. A direct ELISA was conducted with the serum, immunodepleted serum (or "flow-through"), and the purified antibody to check the efficiency of the purification product. These three fractions were initially brought to 1.0mg/ml and then diluted in as given **(Table S6**), and the optical density (OD) readings taken as shown. The gradient dilution of the purified anti-TSPO antibody suggested an immune response to the antigen.

Next, we examined the antibody in tissue or cells from different species. Using this anti-rabbit TSPO antibody in immunoblots, we could detect TSPO as a 36kDa band in human heart lysate (Cat. No.: 1401, ProSci, Inc. CA, USA) (**Fig. S11B**), an 18kDa band in rat adrenal lysate (Cat. No. 1470, ProSci, Inc. CA, USA) (**Fig. S11C**) and an 18kDa band in MA-10 mouse tumor Leydig cells (**Fig. S11D**). With the cell lysate from mouse MA-10 and TSPO KO MA-10 cells (Fan et al., 2018), there is 18kDa band in wild type MA-10 but no expression in TSPO KO MA-10 cells, further confirmation of the knockout of TSPO mediated by CRISPR/CAS9 in MA-10 cells (**Fig. S11E**) and the specificity of the antibody. Using primary hepatocytes from a male C57BL/6 wild type and a male TSPO KO mouse, after probing with TSPO antibody, results showed TSPO expression in wild type but no expression in KO hepatocytes (**Fig. S11F**), indicative of TSPO recognition by the generated TSPO antibody in mouse hepatocytes.

Because TSPO is a resident protein in outer mitochondrial membrane, we examined TSPO distribution in Huh7 cells under confocal laser-scanning microscopy. The results showed that TSPO was localized mainly in the mitochondrial membrane, evidenced by co-staining with MitoTracker (**Fig. S11G**), a mitochondrial maker. In MA-10 cells, we observed TSPO located in the mitochondrial membrane but not detected in TSPO KO MA-10 cells (Fan et al., 2018; **Fig. S11H**). These observations confirmed that the TSPO antibody we generated is applicable to the detection of TSPO in human, mouse, and rat. This TSPO antibody was used for immunofluorescence staining (**Fig. 1B, 2B** and **Fig. S11 G, H**) and immunoblot (**Fig. 7E**) in our present study.

Supplemental References

Hatori, A., Yui, J., Yamasaki, T., Xie, L., Kumata, K., Fujinaga, M., Yoshida, Y., Ogawa, M., Nengaki, N., Kawamura, K*., et al.* (2012). PET imaging of lung inflammation with [18F]FEDAC, a radioligand for translocator protein (18 kDa). PLoS One *7*, e45065.

Ji, B., Maeda, J., Sawada, M., Ono, M., Okauchi, T., Inaji, M., Zhang, M.R., Suzuki, K., Ando, K., Staufenbiel, M*., et al.* (2008). Imaging of Peripheral Benzodiazepine Receptor Expression as Biomarkers of Detrimental versus Beneficial Glial Responses in Mouse Models of Alzheimer's and Other CNS Pathologies. Journal of Neuroscience *28*, 12255-12267.

Li, Y., Lua, I., French, S.W., and Asahina, K. (2016). Role of TGF-beta signaling in differentiation of mesothelial cells to vitamin A-poor hepatic stellate cells in liver fibrosis. Am J Physiol Gastrointest Liver Physiol *310*, G262-272.

Severgnini, M., Sherman, J., Sehgal, A., Jayaprakash, N.K., Aubin, J., Wang, G., Zhang, L., Peng, C.G., Yucius, K., Butler, J*., et al.* (2012). A rapid two-step method for isolation of functional primary mouse hepatocytes: cell characterization and asialoglycoprotein receptor based assay development. Cytotechnology *64*, 187-195.

Sugahara, G., Ishida, Y., Sun, J., Tateno, C., and Saito, T. (2020). Art of Making Artificial Liver: Depicting Human Liver Biology and Diseases in Mice. Semin Liver Dis *40*, 189-212.

Xiong, S., She, H., Zhang, A.S., Wang, J., Mkrtchyan, H., Dynnyk, A., Gordeuk, V.R., French, S.W., Enns, C.A., and Tsukamoto, H. (2008). Hepatic macrophage iron aggravates experimental alcoholic steatohepatitis. Am J Physiol Gastrointest Liver Physiol *295*, G512-521.